Ferroelectric and Dielectric Properties of Poly(vinylidene fluoride) Nanocomposite Films Filled with Iron Oxide Nanoparticles

Karlsruhe Optics and Photonics (KSOP), KIT

Chengcheng Yan

Matriculation No. 1510589

KSOP Advisor: Prof. Dr. rer. nat. Uli Lemmer
Lichttechnisches Institut, KIT

Co-Advisor: Dr. Kamal Asadi, Hamed Sharifi Dehsari
Max Planck Institute for Polymer Research, Mainz

Submitted date: 22. January 2018

Erklärung

Hiermit versichere ich, die vorliegende Arbeit selbständig angefertigt, alle dem Wortlaut order Sinn nach entnommenen Inhalte andere Werke an den entsprechenden Stellen unter Angabe der Quellen kenntlich gemacht und keine weiteren Hilfsmittel verwendet zu haben.

Chengcheng Yan

Karlsruhe, den 22. Januar 2017

Abstract

Polymer-based nanocomposites have attracted much attention in recent years for their outstanding mechanical and electrical properties. Ferroelectric material Polyvinylidene fluoride (PVDF) has been a well-known candidate and had been widely studied. PVDF is semi-crystalline polymer and exists in at least four crystalline phases, called α, δ, β and γ. Electroactive β-phase is highly desirable because of its all trans(TTT) planar zigzag chains conformation, whose dipole components normal to chain axes with largest polarization. There are many papers report the addition of nanofillers such as $BaTiO_3$, $CoFe_2O_4$, $NiFe_2O_4$, carbon nanotube and graphene oxide in PVDF matrix could induce β-phase. However, most of the reported films were fabricated by solvent casting method which thickness is above 20um with high roughness and thin film nanocomposite has not been reported yet. This work is motivated by the idea the incorporation of Fe_3O_4 nanoparticles into PVDF could enhance ferroelectricity and improve dielectric properties.

PVDF: Fe_3O_4 composite films were fabricated by spin coating and wire bar coating respectively. After deposition of the film, samples were subjected to various thermal treatments, such as annealing and melt-quenching followed by annealing. Atomic force microscope (AFM), fourier-transform infrared spectroscopy (FTIR), scanning electron microscopy (SEM), X-ray diffraction (XRD) and differential scanning calorimetry (DSC) were used for the material characterization. Dielectric and hysteretic electric displacement with respect to applied field loop measurements were conducted. The nanocomposites processed by wire bar coating and drop casting show improved dielectric constant at a low loading of Fe_3O_4 nanoparticles. The addition of Fe_3O_4 does not induce β-phase PVDF.

CONTENTS

List of Figures

List of Tables

Chapter 1

1 Introduction

1.1 Multiferroic Magnetoelectric Materials

Multiferroics are attracting much attention for long-term technological applications such as memory devices, actuators and spintronic devices [1]. The definition of multiferroics is the class of materials possessing two or all three ferroic properties: ferroelectricity, ferromagnetism and ferroelasticity. Multiferroic magnetoelectric (ME) materials are defined as materials that posse both ferroelectric and ferromagnetic properties in the same phase [2]. According to material constituents, multiferroic magnetoelectric materials can be classified as two types: single phase materials in which ferromagnetism and ferroelectricity arise independently also coexist, but are rare. Another type is composites which are multiphase materials combining ferroelectric and magnetostrictive components [3]. Polymer-based ME nanocomposites films which consist of both ferroelectric and magnetic orderings have many advantages such as easily processing, lightweight, and less expensive. Figure 1 shows the schematic representation of ME nanocomposites which ferroelectric polymer is used as a matrix and magnetic nanoparticles are used as fillers [4].

Magnetoelectric(ME) coupling describes the influence of a magnetic (electric) field on the polarization (magnetization) of a material. In magnetoelectric materials, ferroelectric polarization can be controlled by an external magnetic field and the magnetization can be controlled by an external electric field [2]. The ME effect in composite materials is a product tensor property which results from the cross

interaction between the two phases in the composite. The composite magnetic effect can be described as follows [5]:

$$Direct\ ME\ effect = \frac{Magnetic}{Mechanical} \times \frac{Mechanical}{Electric} \tag{1}$$

$$Converse\ ME\ effect = \frac{Electric}{Mechanical} \times \frac{Mechanical}{Magnetic} \tag{2}$$

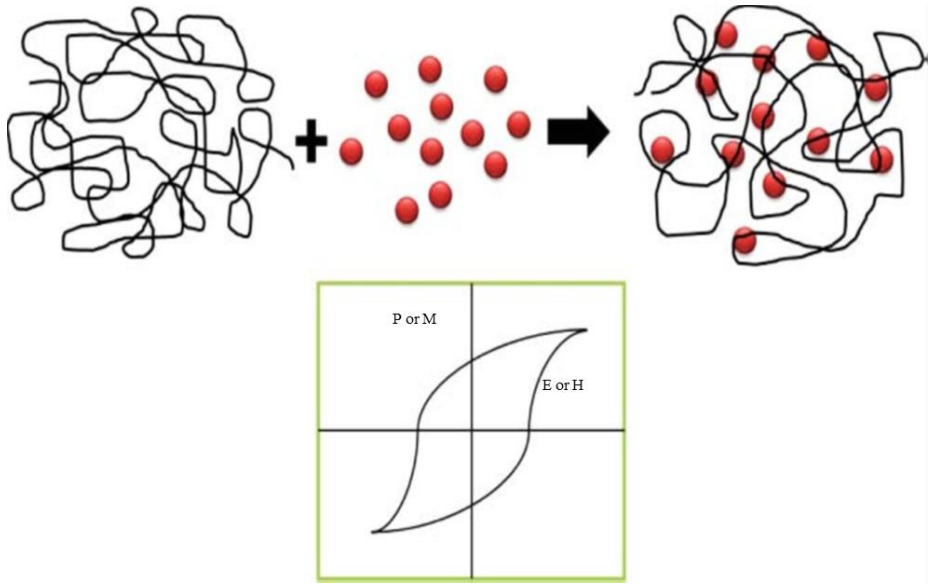

Figure 1. Schematic representation of magnetoelectric nanocomposite and mutual control of polarization (P) and magnetization (M) by electric (E) and magnetization (M) by electric (E) and magnetic fields (H)

1.2 Ferroelectric Materials

A ferroelectric system exhibits spontaneous polarization, and it must be possible to switch to the opposite direction with the reversal of the electric field. The polarization value at zero bias is called the remnant polarization (P_r) and the coercive field (E_c) is defined as the minimum field that is required to switch the full

remnant polarization. The hysteresis loop (electric displacement with respect to applied field) is one of the most common and straightforward tools to characterize ferroelectrics. In general, a ferroelectric film can only be measured when it is fabricated as a device (typically a capacitor). For an ideal linear dielectric, there is a straight line in the D-E loop. For an ideal resistor, an ellipse or a football shape will be presented. For ferroelectric material (Figure 2) [6], when the electric filed is much smaller than coercive field, the measurement shows only a linear electric displacement. And when the field close to the coercive field, the ferroelectric starts to polarize and saturates at high fields. I-V curve measurement can also be used to distinguish ferroelectric switching from artifacts. If the sample is ferroelectric, switching peaks are visible in the I-V curve measured during the switching process. Figure 2 (b) shows switching peaks in a ferroelectric material.

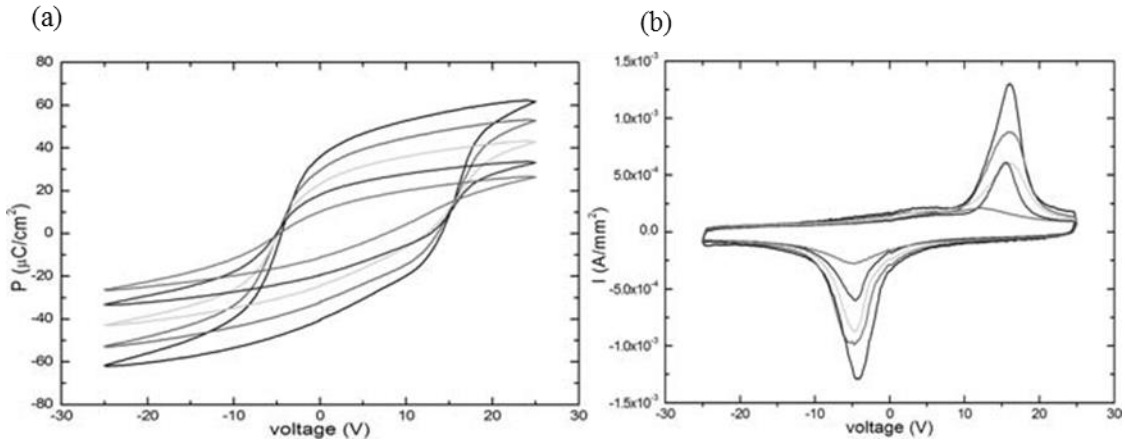

Figure 2. (a) Hysteresis loops for a number of $PbTiO_3/SrTiO_3$ samples. **(b)** The corresponding current–voltage loops.

Polyvinylidene fluoride (PVDF) is one of the most commonly used organic ferroelectric material. Its remarkable properties include high pyroelectric and piezoelectric coefficients, excellent mechanical properties, high dielectric strength, and outstanding chemical stability. These properties have made this polymer a

suitable candidate for many technological applications, such as sensors, actuators and non-volatile memory device [7,8]. PVDF is a semi-crystalline polymer with a chemical formula of $(CH_2–CF_2)_n$ that can crystallize into at least four phases, called α, β, γ, and δ [9]. The nonpolar α phase is most commonly obtained due to its high thermodynamic stability and can usually be produced by crystallization from the melt or from dimethylformamide or dimethylacetamide solutions at temperatures above 120 °C [10]. For α phase PVDF, dipole components normal to the chain axes are antiparallel and the net dipole moment vanishes [4]. Although the dipole moments of α phase are internally vanished, a polar analog, that is δ phase can be obtained by electro-forming [11]. By stepwise increasing electric field, hysteresis starts to appear. When the electric filed reaches to 250 MVm^{-1}, paraelectric α phase PVDF became ferroelectric δ phase. After poling, the ferroelectric properties of PVDF film was fixed. Figure 3 (a) and (b) shows electro-forming process [11].

The electroactive β phase is highly appreciated. Its unit cell consists of two all-trans chains packed with their dipoles pointing in the same direction leading to the highest spontaneous polarization [12]. Strong electric moments in the PVDF monomer unit arise due to stronger electro-negativity of fluorine atoms compared with those of hydrogen and carbon atoms. Thus, each chain has a dipole moment perpendicular to the polymer chain. For polar β phase conformation, the polymer chains pack in crystals to form parallel dipoles, resulting in a net non-zero dipole moment. Figure 3 (c) and (d) present the molecular arrangement of fluorine and hydrogen element with carbon back bone of PVDF polymer chain in α and β phases [4]. The molecular conformation of polar β phase of PVDF is the most important phase for technological applications due to its better ferroelectric, pyroelectric properties and large piezoelectric coefficients. For this reason, increasing β phase content of PVDF matrix has always been an important job. The polar β phase cannot be naturally achieved in film fabrication. Traditionally β phase is obtained by mechanically

stretching non-polar α phase films [13]. However, this method has obvious limitations for electronic applications that usually require the preparation of thin films directly on substrates. An alternative method for the formation of the β phase PVDF is by solvent casting from an appropriate solvent (e.g. from Dimethylformamide) below 70 °C. However, the ferroelectric polymers prepared at low evaporation temperature results in high porosity films and poor electrical and mechanical properties [14].

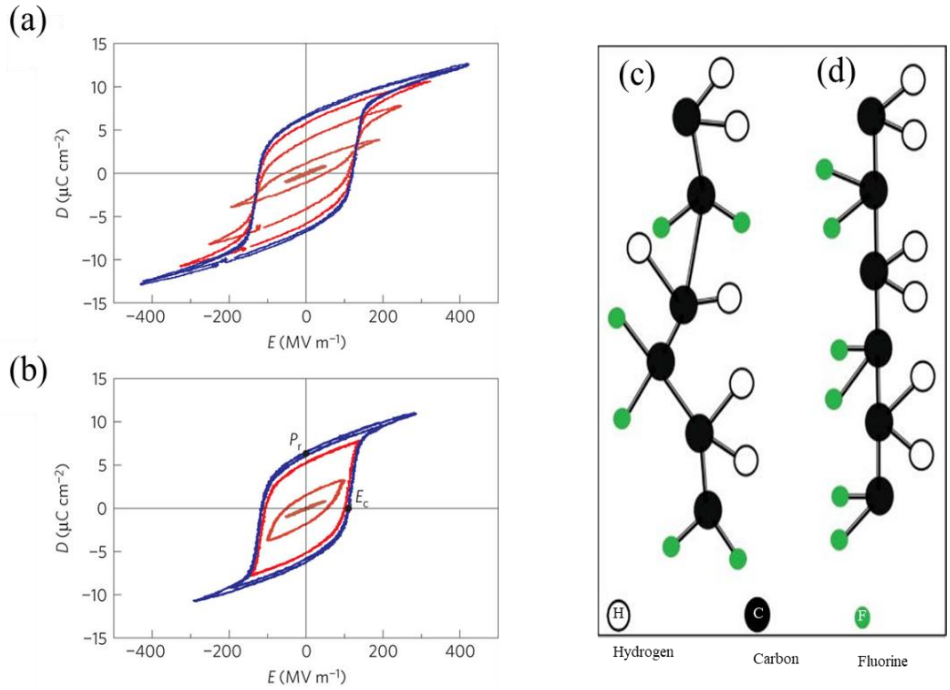

Figure 3. (a) Hysteresis loops during poling. **(b)** Hysteresis loops for the same thin-film capacitor after poling. **(c)** Molecular structure of α phase and **(d)** β phase of PVDF.

There are some papers report the inclusion of nanofillers such as $BaTiO_3$ [15], graphene oxide [16], clay [17] and ferrite nanoparticles [18] in polymer, the electroactive β phase content has been enhanced. However, most of the reported films were fabricated by solvent casting method which thickness is above 20um with high roughness and ferroelectric hysteresis loop has not been exhibited. The possible reason is the PVDF nanocomposite films obtained in this way shows high porosity

leading to poor electrical properties and it is very difficult to give enough voltage to such thick film. PVDF nanocomposite thin films with good electrical properties have not been reported yet. Taking this as an initial point, we add Fe_3O_4 nanoparticles into PVDF polymer to fabricate thin film, investigating the influence of nanoparticles in PVDF polymer matrix.

1.3 Polymer Nanocomposite Dielectrics

PVDF possesses outstanding dielectric properties, such as high permittivity, high breakdown strength and relatively low dielectric loss that makes it a suitable candidate for applications in high energy density storage [19]. However, the intrinsic low dielectric constant values (<10) of polymer materials restricts their developments into industry. The introduction of inorganic nanoparticles into an insulating polymer is an important approach to enhance the overall dielectric constant. Table 1.1 summarize the dielectric properties of polymer composites as reported in the literature. Ceramic materials of large permittivity such as $BaTiO_3$ is most commonly used. However, high volume fraction (>50 vol%) of ceramics was needed to achieve the high dielectric constant and the resulting material suffers from low flexibility, low electrical breakdown strength and poor mechanical performance [20]. By adding conductive nanofiller such as graphene nanoribbon (GNR), the dielectric constant can be greatly enhanced. However, conductive filler nanocomposites always exhibit very high dielectric loss due to the insulator–conductor transition occurring at the percolation threshold [21].

Nano-sized ferrites have gained much attention due to their interesting surface reactivity, electrical and magnetic properties [22]. In this work, Fe_3O_4 was chosen as the nanofiller due to its large magnetostrictive coefficient value [4], which can act as

excellent candidate for the magnetic phase for the further magnetoelectric coupling study.

Host polymer	Filler material	Dielectric constant (1 kHz)	References
PVDF	$CoFe_2O_4$ (5 wt %)	11.2	[3]
PVDF	$Na_xTi_yNi_{1-x-y}O$	600–750	[23]
PVDF	Carbon coated boron nitride (30 vol %)	39	[24]
PVDF	$CaCu_3Ti_4O_{12}$ (30 vol %)	90	[25]
PVDF	BT–Fe_3O_4 (33 vol %)	385	[26]
P(VDF-HFP)	$BaTiO_3$ (BT) (50 vol %)	48	[27]
PVDF	(PVP)-encapsulated Au (12.5 wt %)	22	[28]
PVDF	$La_{1.7}Sr_{0.3}NiO_4$ (35 wt %)	3285	[29]
PVDF	exfoliated graphite nanoplates	200	[30]
PVDF	Ag (20 vol %)	120	[31]
PVDF	nanocrystalline nickel	2050	[32]
PVDF	TiO_2@MWCNTs (1 wt %)	50	[20]
PVDF	$BaFe_{12}O_{19}$ (12 vol %)	60	[33]
PVDF	$BaTiO_3$ (40 vol%)	65	[34]
PVDF	TiC (11.58 vol%)	540	[35]

Table 1. Dielectric constant of polymer nanocomposites as reported in the literature.

1.4 Thesis Outline

The introductory chapter has presented the motivation and background of PVDF nanocomposites. The next chapter describe nanocomposite preparation, film fabrication and material characterization techniques. In chapter 3, the influence of processing conditions is discussed, and the suitable processing parameters are selected for the further device fabrication. Chapter 4 presents PVDF: Fe_3O_4 nanocomposite thin films fabrication, followed by the detailed characterization of the nanocomposite. In chapter 5, nanocomposite thick films are investigated, including morphology, material and electrical characterization. Chapter 6 summarizes the thesis and presents the outlook.

Chapter 2

2 Experimental

2.1 Materials

Poly(vinylidene fluoride) (PVDF)(M_w 180 and 275 kg/mol) was supplied in pellet form by Sigma-Aldrich and was used as received. N,N-dimethylformamide (DMF, pure grade) was used as solvent. Fe_3O_4 magnetic nanoparticles with average diameter 11 nm were used in this work and synthesized by Hamed Sharifi Dehsari. The corresponding synthesis method of Fe_3O_4 nanoparticles can be found in report [36, 37].

2.2 PVDF: Fe_3O_4 Nanocomposite Preparation

The synthesized Fe_3O_4 nanoparticles were initially dissolved and saved in toluene. In order to separate Fe_3O_4 nanoparticles, antisolvent ethanol was used to mix with toluene solution, typically in 1:3 ratio by volume. Then shaking the mixed solution and put the solution next to the magnet, since Fe_3O_4 nanoparticles have magnetic properties, Fe_3O_4 nanoparticles would attach to the vial' wall and separate from liquid. Finally, the colorless liquid was discarded by pipette and then Fe_3O_4 nanoparticles were dried in vacuum oven at 60 °C overnight.

We use solution-mixing method to prepare nanocomposite solution. PVDF pellets were dissolved in N,N dimethylformamide(DMF) through magnetic stirring at a temperature around 100 °C for 2 hours to ensure wholly dissolution. Separately, the desired amount of dry Fe_3O_4 nanoparticle power was add to DMF solvent followed by ultrasonic stirring for 4 hours to get a homogenous dispersion. PVDF: Fe_3O_4

composite solution was obtained by directly mixing the polymer solution with nanoparticle suspension under continuous ultrasonication for 6 hours.

2.3 Film Deposition

Deposition of thin films from solutions can be achieved by several approaches, including spin coating, wire bar coating and solution casting. In the polymer solution casting method, nanocomposite solution is directly dropped onto the substrate, and then the solvent evaporates spontaneously, allowing film formation. The produced film may be stripped from the substrate and to get a free-standing film. However, the coating across the surface is usually poor uniformity and it is hard to control film thickness.

Spin coating is one of the most common techniques used to produce uniform thin films on substrates. By applying the solution onto the center of a substrate and then rotating the substrate at a certain spinning speed, the fluid flows outward radially by centrifugal force. The final film thickness depends on many controllable parameters such as solution viscosity, rotational speed and solution concentration. Figure 4 shows a schematic of the spin coating method [30].

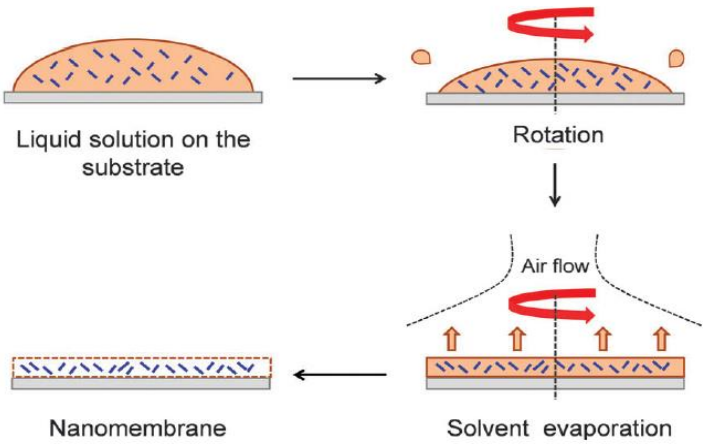

Figure 4. Schematic to illustrate the spin coating process

Wire-bar coating is widely used in large-area fabrication of organic films at low cost. A typical wire-bar machine employs a wire wound bar above a substrate (Figure 5). The coating process includes the following steps. (1) A sufficient polymer solution is introduced into the space next to the front edge of wire wound bar. (2) The wire bar moves at a controlled speed against the fixed substrate. (3) The solution layer is spread evenly on the substrate. The heated bed which has a smooth aluminum face under substrate could be used to adjust the evaporation of the solvent. The concentration of polymer solution, the dimension of the wires wound on the wire-bar, velocity and heating temperature determine the final thickness of the film.

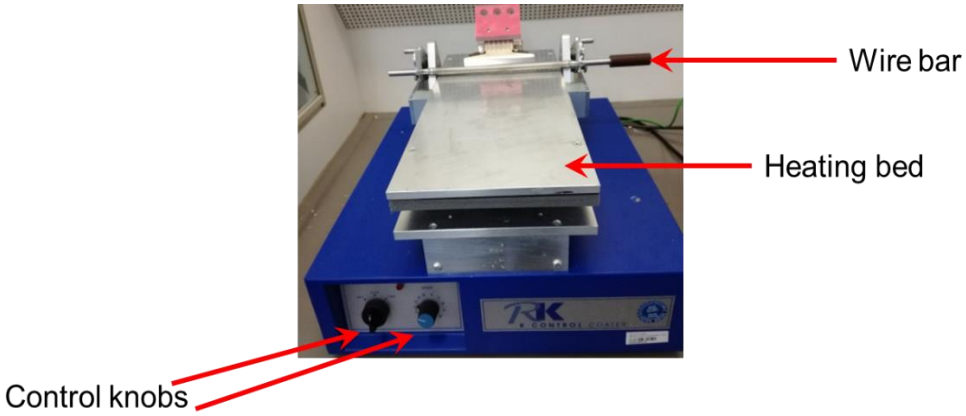

Figure 5. K102 K Control Coater from RK PrintCoat

2.4 Material Characterization

2.4.1 Atomic Force Microscopy (AFM)

Nanoscope Dimension 3100 Bruker Atomic Force Microscopy was used to study the surface morphology of the nanocomposite films. AFMs operate by measuring interaction force between a probe and the sample. When the tip approaches the sample surface, attractive forces act upon the tip causing the cantilever to deflect towards the surface. When the tip is in contact with the surface, increasingly

repulsive force takes over according to Hooke's law. The beam deflection method is used to detect cantilever deflections towards or away from the surface. A position sensitive detector can be used to track probe motion change and has to be calibrated into electrical signal and the topographic map of the sample surface features can be generated.

2.4.2 Fourier Transform Infrared Spectroscopy (FTIR)

The phase identification of nanocomposite film was analyzed by Fourier transform infrared (FTIR) spectroscopy. FTIR spectra were recorded using a Bruker Tensor II FTIR spectrometer at a spectral resolution of 4 cm^{-1}. In FTIR analyses, Infrared light from the light source passes the sample through the interferometer and reaches the detector. Then the signal is converted to digital signal which is transferred to a computer and Fourier transform is performed. Since chemical structures (molecules) produce specific IR fingerprints, the FTIR spectra with pattern provide sample structural information.

2.5 Electrical Characterization

2.5.1 Sawyer-Tower Circuit

Dielectric displacement loops versus electrical field (D-E loop) measurements were carried out using Sawyer-Tower circuit. The electric circuit is shown in Figure 6 [38] . Ferroelectric sample and a reference capacitor of a well-defined capacitance are connected in series and therefore carry the same charge. In order to generate D-E loop at oscilloscope, a voltage that is proportional to the electric filed of the ferroelectric sample at the x-channel and a voltage proportional to the dielectric displacement of the sample at the y-channel are needed. Since capacity of reference capacitor is high enough in comparison to the ferroelectric sample capacity, we do not need to take voltage drop at reference capacitor into account. That means that

the voltage at ferroelectric sample is almost equal to the supply voltage which can be read from x-channel. At the same time, the oscilloscope is connected to measure the voltage across the reference capacitor, the polarization of the ferroelectric sample is proportional to the voltage of y-channel. and the P-E loop can be easily obtained. The ferroelectric samples were measured with a continuous triangular wave signal at a frequency of 100 Hz, using a reference capacitor of 220 nF.

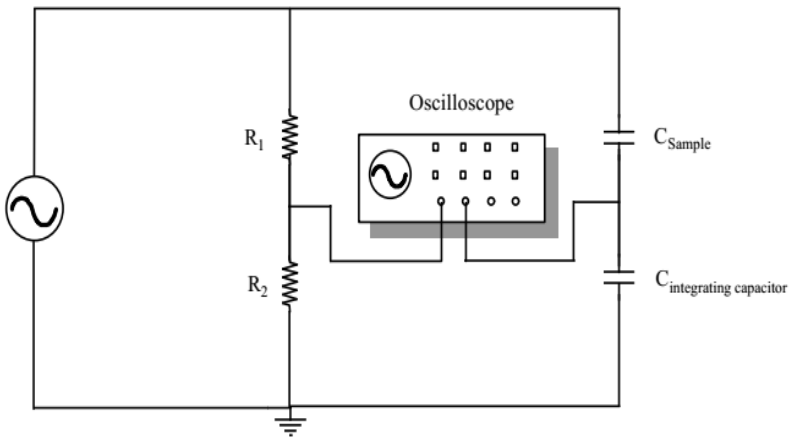

Figure 6. Schematic of a Sawyer Tower circuit for P-E loop measurements.

2.5.2 Dielectric Spectroscopy

Dielectric properties were characterized using a Novocontrol spectrometer with a frequency sweep from 0.1 Hz to 10 MHz. Dielectric spectroscopy measures the dielectric permittivity as a function of frequency. The material permittivity is a complex number, which consists of a real part ε' and an imaginary part ε". ε' is a measure of the energy stored whereas ε" is a measure of energy loss. Another useful quantity is the loss factor

$$\tan\delta = \frac{\varepsilon''}{\varepsilon'} \tag{3}$$

The term tanδ is called loss tangent and loss angle δ is correlated with impedance phase angle θ, for a lossless capacitor, voltage drop always lags current by 90°, so

the impedance phase angle is -90° and tanδ is 0. But because of material absorption, the impedance phase angle of the real capacitor is

$$\theta = -(90 - \delta) \tag{4}$$

Chapter 3

3 PVDF Thin Film Processing

Ferroelectric polymer thin films for micro-electronic applications require high-quality films with transparent and smooth surfaces. However, PVDF thin films prepared at room temperature and at relative humidities greater than 25% possessed a cloudy appearance and a rough surface [39, 40] which were hard for electric characterization. In this chapter the processing condition for polyvinylidene fluoride (PVDF) thin film was investigated. Experimental results indicate that PVDF film qualities are affected by deposition temperature. At high deposition temperature, PVDF thin films presented low roughness.

3.1 Spin coated PVDF Thin Films

PVDF solutions were prepared by dissolving PVDF pellets (Mw = 180 000 g/mol, Sigma-Aldrich) in N,N-dimethylformamide (DMF) with a magnetic stirrer at 100°C for 2 hours to get transparent solutions. The PVDF concentration was 50 mg/ml. Thin films were prepared by spin coating (spinning speed, acceleration and time of 3000 rpm, 3000rpm s^{-1} and 60s, respectively) onto thoroughly cleaned glass substrates an elevated temperature in ambient air. These substrates were rinsed with distilled water, acetone, isopropanol and dried with nitrogen. Prior to use, the substrates were further applied a UV-ozone treatment for 10 minutes to remove contamination and improve wetting ability. The substrates were heated by a heat gun and the temperature was detected by an infrared thermometer (RS 1327K). The morphology and roughness of films were characterized by atomic force microscopy (AFM), DEKTAK surface profilometer was used to measure film thicknesses.

Figure 3.1 shows the AFM images of PVDF thin films (Figures 7 a-e) and the thickness and roughness (Figure 7 f) as a function of deposition temperature. It was found that average thickness of coated film increases with increasing deposition temperature, which could be due to the increased solution viscosity at high temperature. It should be noted that the roughness of coated film is around 10 nm even the film thickness increases. The experimental results indicate that PVDF thin films with smooth and flat surface can be obtained at high deposition temperature by spin coating method.

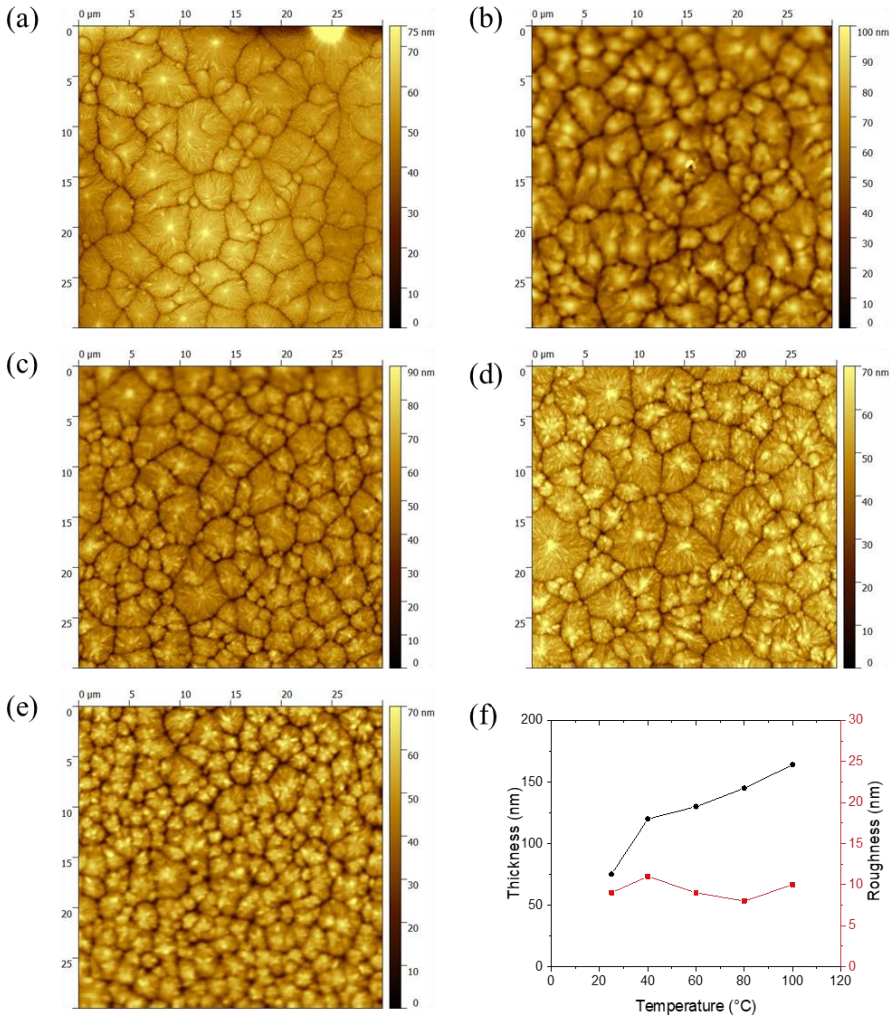

Figure 7. AFM images of PVDF thin films spin coated at: (**a**) 25 °C, (**b**) 40 °C, (**c**) 60 °C, (**d**) 80 °C, (**e**) 100 °C; and (**f**) thickness and roughness as a function of temperature. The solution concentration is 50 mg/ml in DMF.

The influence of solution concentration and spinning speed on the thickness of PVDF thin films deposited by spin coating at about 100 °C was studied. Figure 8 exhibits the effects of spinning speed and solution concentration on the PVDF film thickness and roughness. The average thickness of coated film increases with decreasing spinning speed and increasing solution concentration; however, the roughness of PVDF films increase simultaneously, which means the film surface profile becomes less smooth. To obtain thickness of film around 300nm with corresponding roughness around 15nm, PVDF solution concentration at 75mg/ml with spinning speed at 3000 rpm are suitable parameters for further device fabrication.

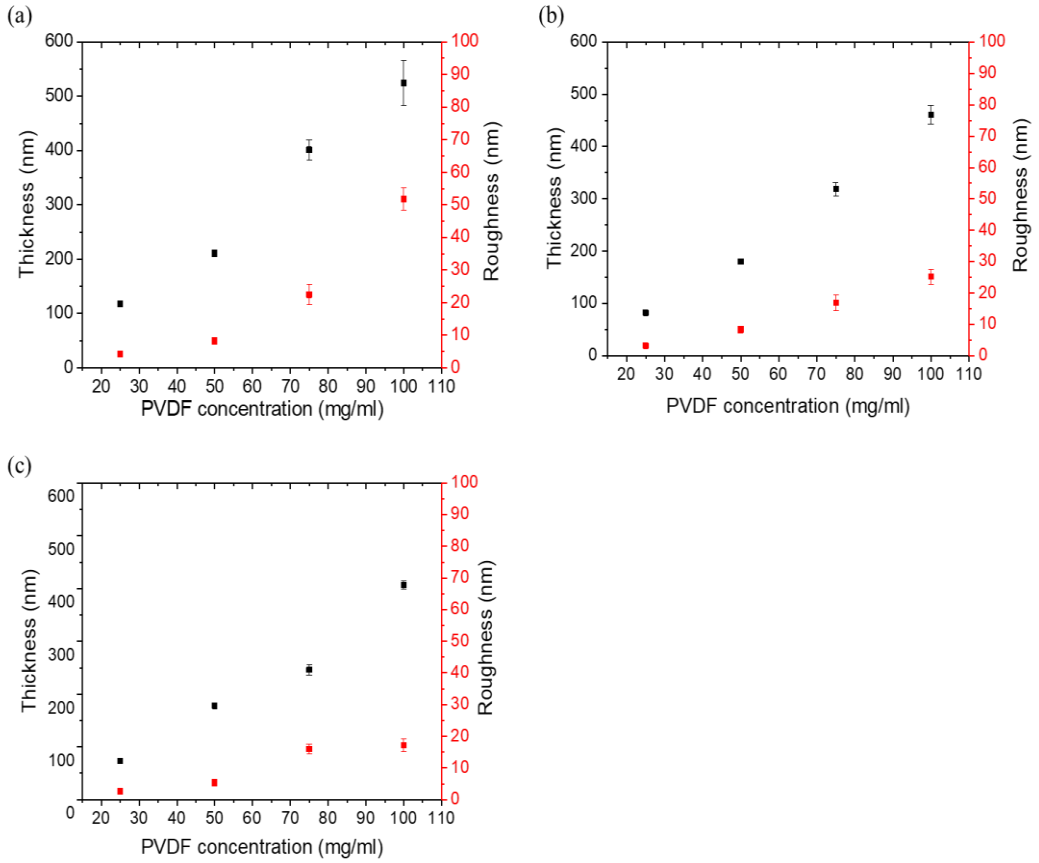

Figure 8. The film thickness and roughness as a function of solution concentration. (**a**) 2000 rpm, 2000 rpm s^{-1}. (**b**) 3000 rpm, 3000 rpm s^{-1} and (**c**) 4000 rpm, 4000 rpm s^{-1}. The spinning duration for each sample is 60s.

3.2 Wire-bar coated PVDF Thin Films

Wire-bar coating is a mature deposition technique [2], which could control deposition temperature accurately. PVDF thin films were prepared by wire-bar coating with solution concentration at 75 mg/ml and 5% relative humidity. The substrates temperature was controlled by the heated bed below the substrates. The surface morphologies of PVDF films with different deposition temperature are shown in Figure 9.

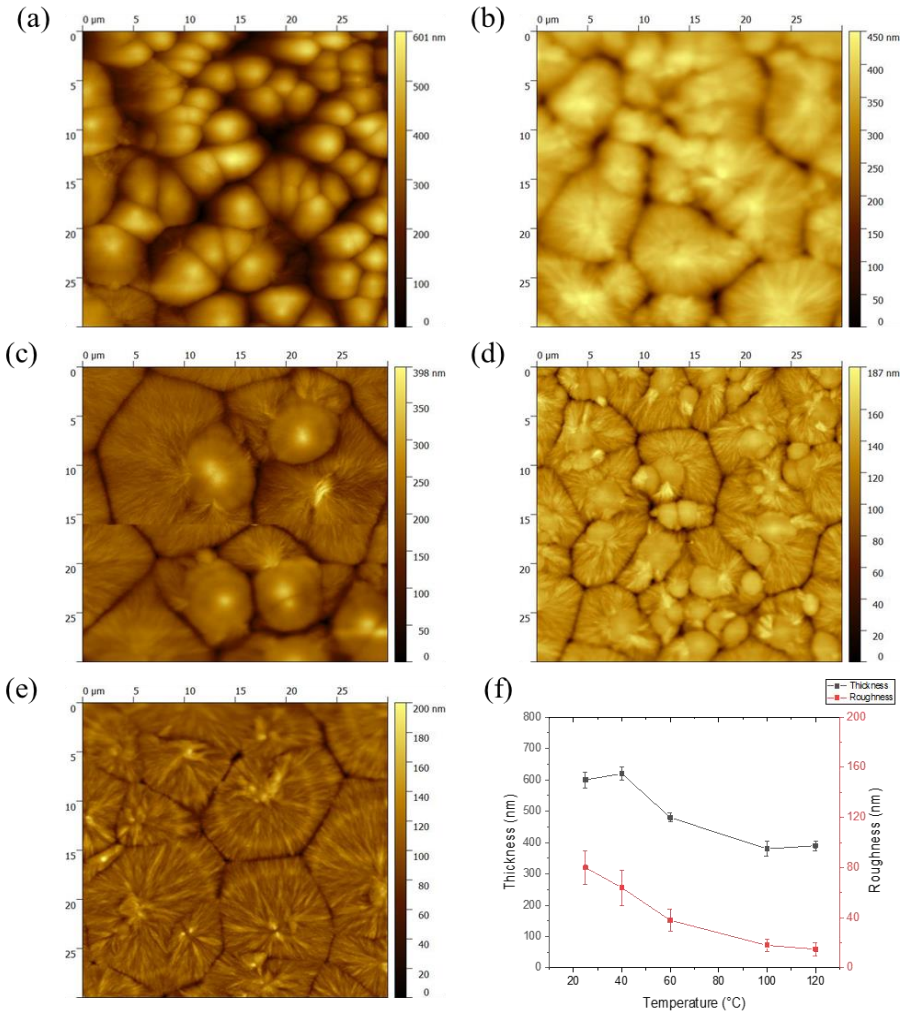

Figure 9. AFM images of PVDF thin films wire-bar coated at: (**a**) 25 °C, (**b**) 40 °C, (**c**) 60 °C, (**d**) 100°C, (**e**) 120°C; and (**f**) thickness and roughness as a function of temperature. The solution concentration is 75 mg/ml in DMF.

It was revealed that the difference in film quality at different deposition temperature. At room temperature, the films with porous structure because of the slower evaporation rate of DMF. The morphology changed substantially after increasing deposition temperature. The high deposition temperature increases solvent evaporation rate, leading films with a dense and smooth surface. It is also to notice the thickness and roughness difference at different deposition temperature. The film thickness and roughness systematically decrease with increasing deposition temperature. We chose PVDF film preparation temperature at 100 °C for further study.

The relationship between film thickness and the solution concentration together with the diameter of the wire was investigated. The films were prepared at 100 °C and 5% relative humidity. Figure 10 shows the thickness and roughness change as a function of solution concentration with different wire diameters (Figure 10 (a) US 5 and (b) US 4).

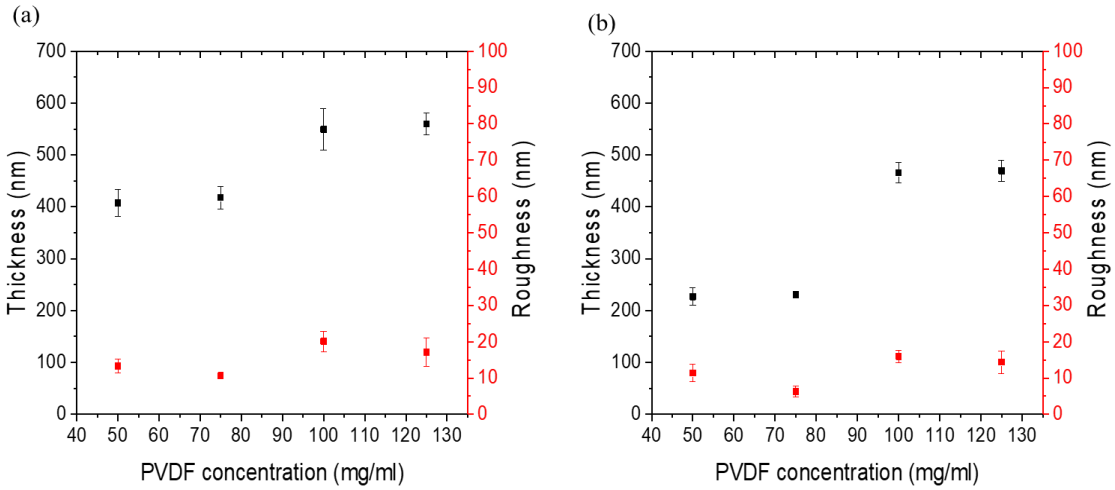

Figure 10. The film thickness and roughness as a function of solution concentration. (a) US 5 and (b) US 4.

3.3 Summary

The effect of deposition temperature and coating parameters (spin coating and wire-bar coating) for PVDF thin films were investigated. It was revealed that the quality of films prepared at an elevated temperature was significantly improved. Porosity is greatly eliminated compared to those prepared at room temperature. For thin film device fabrication, the desired thickness is around 300 nm. From our experimental result, spin coating at 100 °C is suitable for device fabrication to achieve transparent and smooth surface with low roughness.

Chapter 4

4 PVDF: Fe_3O_4 Nanocomposite Thin Films

In this chapter, we systematically investigated the morphology and physical properties including ferroelectric properties and dielectric properties of PVDF nanocomposite thin film containing Fe_3O_4 nanoparticles. The size and crystal structure of the synthesized Fe_3O_4 nanoparticles were characterized using transmission electron microscopy (TEM) and X-ray diffraction (XRD) respectively. Scanning electron microscopy (SEM) and atomic force microscopy (AFM) were performed to analyze the dispersion of synthesized Fe_3O_4 nanoparticles in polymer matrix and microstructural feature.

4.1 Experimental process

4.1.1 Synthesis of Fe_3O_4 Nanoparticles

The magnetic nanoparticle synthesis was performed by using the method reported in [36, 37]. The size distribution and form of the Fe_3O_4 nanoparticles were analyzed with transmission electron microscope (Figure 11 a). TEM images reveal nanoparticles average size about 11 nm. Figure 11 b presents the XRD patterns of the as-synthesized nanoparticles. The diffraction patterns and the intensities could be indexed to an inverse spinel structure with a high degree of crystallinity [36, 37]. The narrow sharp peaks indicate the high purity of the synthesized nanoparticles.

4.1.2 PVDF: Fe_3O_4 Nanocomposite

Nanocomposite films of PVDF: Fe_3O_4 with nanoparticle concentrations of 1, 4, 7, 10, 15, 30, 50% (w/w) and an average thickness of 300 nm were prepared by spin

coating at 100 °C. Initially, certain amount dried Fe_3O_4 nanoparticle powder was dispersed in DMF and placed in an ultrasound bath for 6 hours. Separately, certain amount PVDF pellets were added to DMF under magnetic stirring and heated at 100 °C for 2 hours and then filtered with 1 um filter to form a clear solution. The polymer solution concentration is 75 mg/ml. Nanocomposite suspension was prepared by directly blending the particle suspension with polymer solution. The final mixtures were ultra-sonicated for 4 hours.

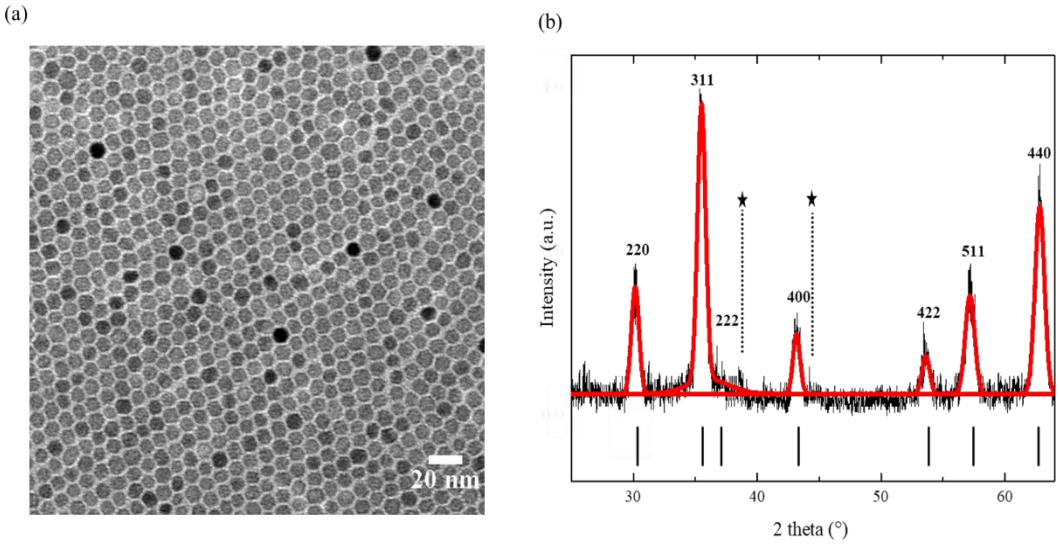

Figure 11. (**a**) TEM image of nanoparticles. (**b**) XRD patterns of the standard reference nanoparticles (black line) and the corresponding modeling result (solid red line).

4.1.3 Capacitor Device Fabrication

5×5 matrix architecture which is also known as cross-bar type capacitor devices were developed (Figure 12). Firstly, 1 nm thick chromium (Cr) was deposited on a clean glass substrate to improve adhesion property. A Gold (Au) layer was evaporated (50 nm) through shadow mask of width 400 µm which acts as the bottom electrode. Nanocomposite films were spin coated on the bottom electrode from the resulting nanocomposite suspension. In order to identify the appropriate thermal processing conditions, the as-casted nanocomposite films were applied further

thermal treatment, including annealing and melt-quenching and annealing. For annealing, the coated films were annealed at 150 °C in a vacuum oven for 2 h and the samples are designated as AN. While for melt-quenching and annealing, the as-cast nanocomposite films were first melt at 200 °C for 2h, and then quenched into the iced water, and in the end annealed at 150 °C for 2h under vacuum. These samples are designated as MQ-AN. The as-cast samples without any further thermal treatment designated as Normal. For the top electrode of the capacitor, Au (50nm thick) was evaporated using a shadow mask. The area of fabricated capacitor is 0,16mm^2.

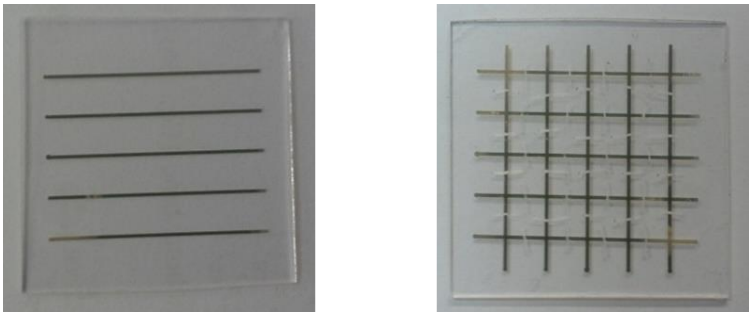

Figure 12. Architecture of capacitor device on a glass substrate.

4.2 Morphology of PVDF Nanocomposite Thin Films

Nanocomposite film quality and uniformity were checked using atomic force microscopy (AFM, Nanoscope Dimension 3100 Bruker). Figure 13 a-c present AFM height images of PVDF: Fe_3O_4 nanocomposite (1 wt %) films with different thermal treatment. Figure 13 d shows the AFM phase image of the corresponding PVDF: Fe_3O_4 nanocomposite (1 wt %) films after melt-quenching and annealing. The films were smooth with flat surface. However, when the concentration of nanoparticles increases to 4 wt %, aggregation occurred (Figure 13 e and f). Large scale SEM measurements also confirm this finding.

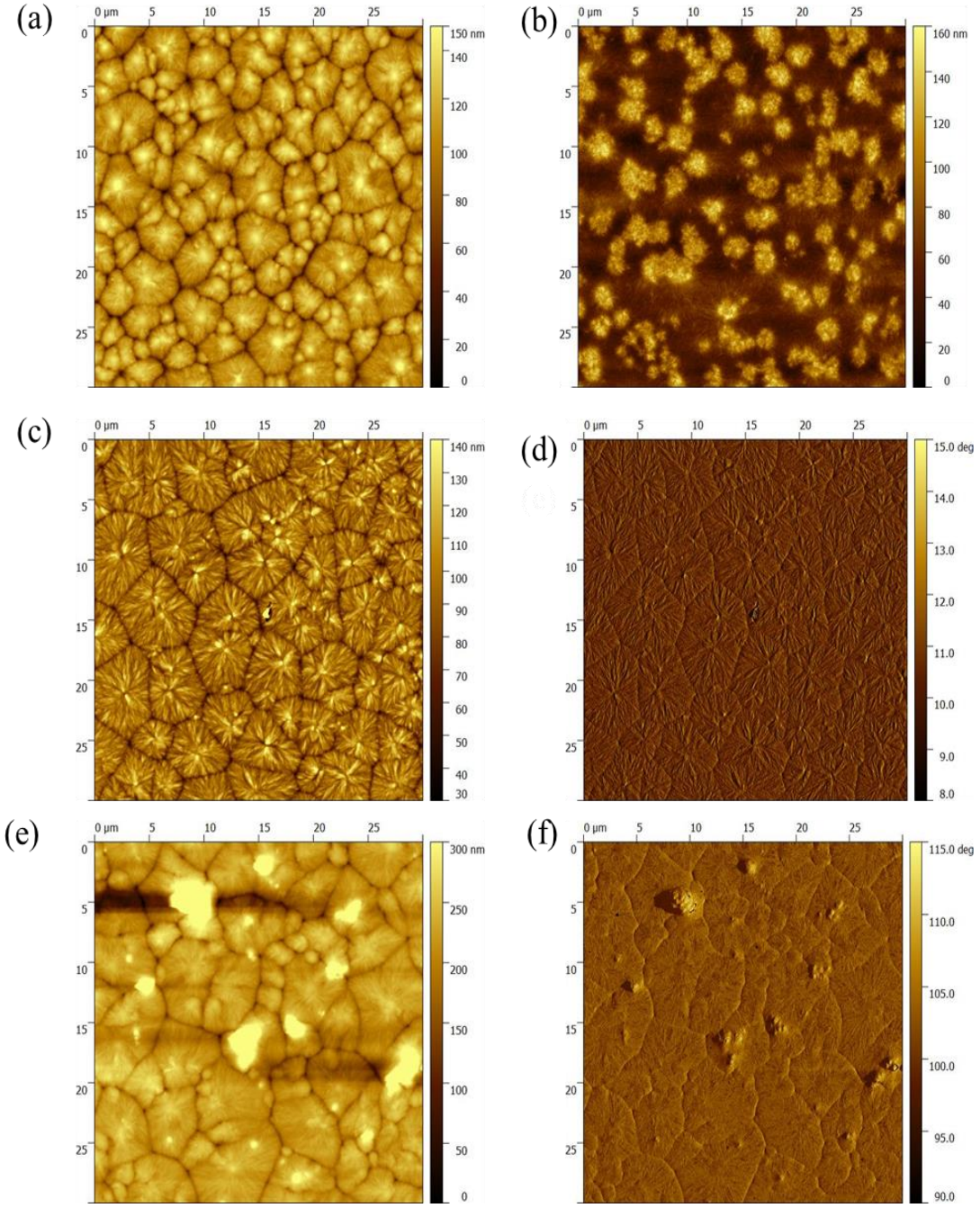

Figure 13. AFM images of nanocomposite films. (**a**) The height image of PVDF: Fe_3O_4 nanocomposite film with 1 wt % nanoparticle content without further thermal treatment. (**b**) The height image of PVDF: Fe_3O_4 nanocomposite film with 1 wt % nanoparticle content after annealing. (**c**) and (**d**) The height and phase images of PVDF: Fe_3O_4 nanocomposite film with 1 wt % nanoparticle content after melt-quenching and annealing. (**e**) and (**f**) The height and phase images of PVDF: Fe3O4 nanocomposite film with 1 wt % nanoparticle content without further thermal treatment respectively.

4.3 Ferroelectric Properties of PVDF: Fe_3O_4 Thin Films

The room temperature ferroelectric (D-E) hysteresis loops based on Sawyer-Tower circuit of pure PVDF and PVDF: Fe_3O_4 composite thin films are shown in Figure 14. The measurements were made at 100 Hz frequency and each measurement was repeated several times to validate the accuracy.

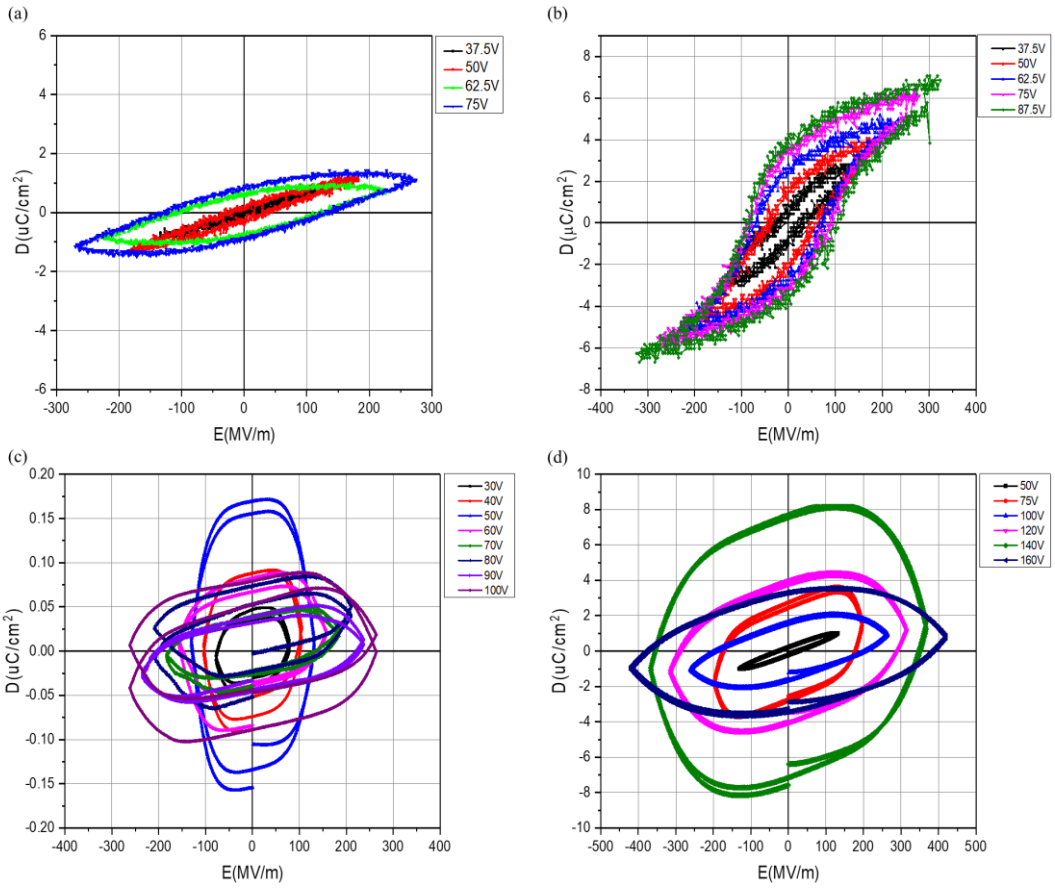

Figure 14. Ferroelectric hysteresis loop. (**a**) Pure PVDF thin film during poling and (**b**) after poling. (**c**) and (**d**) PVDF: Fe_3O_4 nanocomposite thin films with 1 wt % and 4 wt % nanoparticle contents respectively.

It could be observed from the figure that all samples both as-cast samples and after further heat treatment were paraelectric (Figure 14 a). After applying a high electric field of about 250 MV/m, the samples became ferroelectric (Figure 14 b). However,

significant change in polarization was observed for Fe_3O_4 loaded samples. Even for 1 wt% nanoparticles added, the D-E loop became rounded and dielectric leakage increased. At the same time, δ phase could not be induced anymore. For high concentration of nanoparticles, electric breakdown filed reduces dramatically. One of the possible reason is the rotation of molecular chain was prohibited due to the existence of nanoparticles inside of polymer matrix. Another possible reason is the resistivity of Fe_3O_4 is 0.01 Ohm cm at room temperature and present metallic character [42]. Therefore, the addition of Fe_3O_4 nanoparticles decreases the overall resistivity in the system. Moreover, there are some oxygen vacancies in Fe_3O_4 could also lead to the increase of leakage current [43].

4.3 Dielectric Properties of PVDF: Fe_3O_4 Thin Films

In Figure 15, average dielectric constant values were plotted versus nanoparticle concentration for nanocomposite at room temperature and atmospheric pressure 1k Hz. The error bars in Figure 15 represent one standard deviation of the mean dielectric constant. As shown no significant enhancement of dielectric constant has been observed. When the loading of nanoparticles reaches to 15 wt %, the dielectric constant of PVDF nanocomposite films shows a decreasing trend. One of possible reason could be some portion of the Fe_3O_4 nanoparticles have agglomerated into clusters which cause more defects in polymer matrix and affect the performance of the nanocomposite thin films. At the same time, a great amount of naked Fe_3O_4 nanoparticles on the surface were observed in PVDF: Fe_3O_4 nanocomposite thin films by AFM, implying the absence of specific interfacial interaction between Fe_3O_4 nanoparticles and PVDF chains [20]. Another possible reason is the PVDF nanocomposite dielectric constant is a volume average of those of the constituents [44]. However, the dielectric constant of PVDF and Fe_3O_4 are around 8 and 6 respectively, resulting in no increase in the dielectric constant of composites.

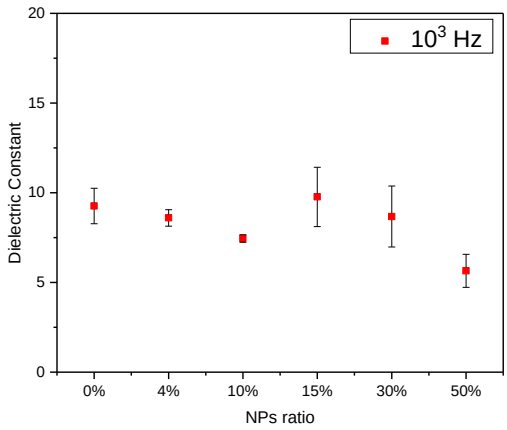

Figure 15. Average dielectric constant of PVDF: Fe_3O_4 nanocomposite films as a function of composition at 10^3 Hz.

4.4 Summary

PVDF: Fe_3O_4 composite thin films have been prepared by spin coating at 100 °C. The addition of Fe_3O_4 nanoparticles does not enhance ferroelectric properties, neither dielectric properties. The possible reason is Fe_3O_4 nanoparticles aggregate, which results in non-uniformity in microstructure and deteriorate the properties of the PVDF nanocomposite.

Chapter 5

5 PVDF: Fe_3O_4 Nanocomposite Thick Films

This chapter reports on the design and development of PVDF: Fe_3O_4 nanocomposite thick films fabricated by wire-bar coating and drop casting respectively. The effects of Fe_3O_4 nanoparticle content on the structural, crystalline phase, thermal, ferroelectric properties and dielectric properties in PVDF matrix were discussed. The PVDF: Fe_3O_4 nanocomposite thick films exhibit composition-dependent dielectric properties. A high dielectric constant accompanied with low dielectric loss upon addition of 5 wt % Fe_3O_4 nanoparticles to PVDF has been observed. Nearly 62% increase of dielectric constant was observed in PVDF: Fe_3O_4 nanocomposite films as compared to pure PVDF films prepared under identical conditions. Fourier transformed infrared spectroscopy (FTIR) and X-ray diffraction (XRD) results reveal that the inclusion of Fe_3O_4 nanoparticles does not affect the PVDF crystalline phase, the processing conditions being the main reason for the formation of the α- or β-phase.

5.1 Wire-bar Coated PVDF Nanocomposite Thick Films

The PVDF: Fe_3O_4 nanocomposite suspension was prepared by using the same method described in chapter 4. PVDF polymer (Mw = 275 000 g/mol, Sigma-Aldrich) was used and the solution concentration is 150 mg/ml. PVDF nanocomposite thick films were prepared by a wire-bar coating deposition method at 95 °C, using a K102 K Control Coater from RK Print Coat Instruments Ltd. The thickness of the obtained thick films was controlled by the dimension of the wires wound on the wire-bar. The coated films were melt at 200 °C for 2h in a vacuum oven and then quenched in ice water and subsequent annealed at 150 °C for 2h.

5.1.1 Morphology Characterization

To study the influence of Fe_3O_4 nanoparticles on the PVDF microstructure, AFM height images of nanocomposite films were presented in Figure 16. At low ratio of Fe_3O_4 nanoparticles (Figure 16 a-c), significant change was not observed. However, when the ratio of Fe_3O_4 nanoparticles reaches to 5 wt % (Figure 16 d), aggregation was observed. Moreover, the roughness of the film increased.

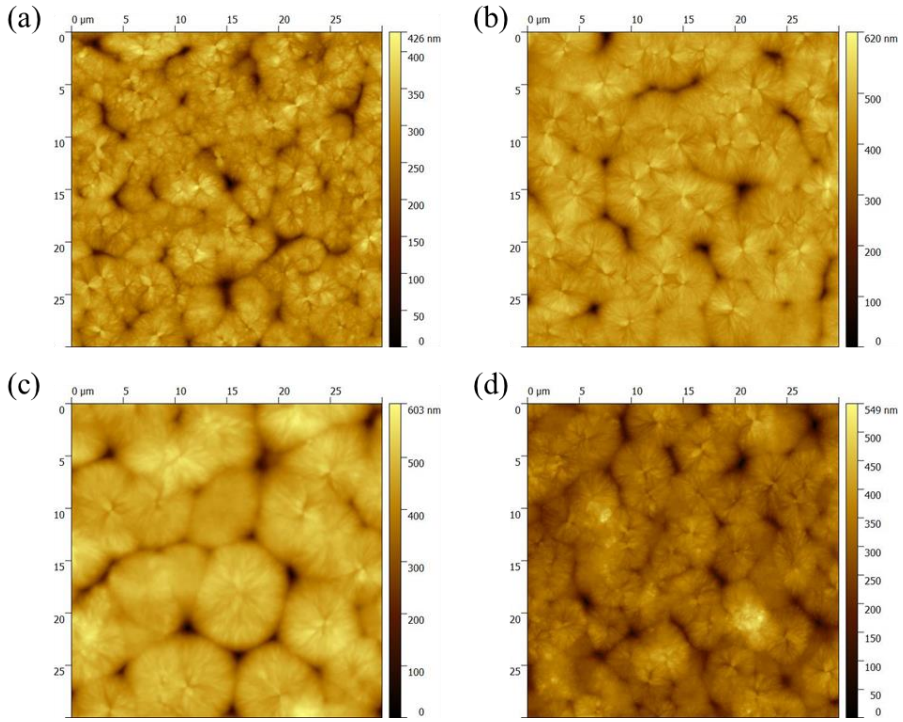

Figure 16. AFM height images. (**a**) Pure PVDF film. (**b**)**,** (**c**) and (**d**) PVDF nanocomposite films with 1 wt %, 3 wt % and 5 wt % nanoparticle contents respectively.

To further verify the PVDF nanocomposite microstructure, the sample (5 wt %) was studied by SEM (Figure 17). The top surface view of the microstructure of the PVDF: Fe_3O_4 nanocomposite film demonstrates that few naked Fe_3O_4 nanoparticles on the surface can be observed as they are encapsulated by PVDF chains, implying that there exist strong interactions between Fe_3O_4 nanoparticles and PVDF chains. The cross-sectional (Figure 17 b) image reveals agglomeration occurs due to the magnetic interaction among nanoparticles.

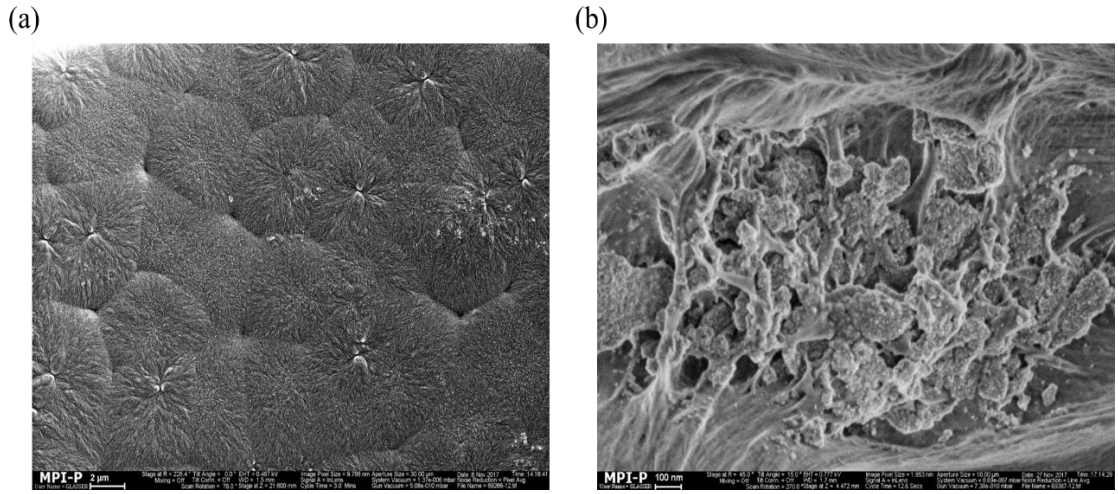

Figure 17. SEM images of 5 wt % PVDF nanocomposite film. (**a**) Top surface view and (**b**) cross-sectional view.

5.1.2 Fourier Transformed Infrared Spectroscopy

The FTIR spectrum of the films provides information about their structure that enables us to distinguish the different crystalline phases of PVDF. Figure 18 shows the FTIR absorption spectra of PVDF and PVDF: Fe_3O_4 nanocomposite thick films. Measurements were carried out using Bruker Tensor II FTIR spectrometer in absorbance mode with at a spectral resolution of 4 cm^{-1} and spectra wavenumber range between 1500 and 400 cm^{-1}. In the FTIR spectrum of pure PVDF, the characteristic absorbance bands at 410 cm^{-1}, 489 cm^{-1}, 532 cm^{-1}, 614 cm^{-1}, 763 cm^{-1}, 795 cm^{-1}, 854 cm^{-1}, 975 cm^{-1}, 1149 cm^{-1}, 1209 cm^{-1}, 1383 cm^{-1} and 1423 cm^{-1} are corresponding to the α phase [45]. In the case of Fe_3O_4 nanoparticles added to PVDF, all the samples show the same typical α phase characteristic peaks as pure PVDF without any β or γ phase. α phase PVDF is easily distinguished and in our case, wire-bar coated samples all show characteristic perks of α phase. There are only two exclusive bands of 1275 cm^{-1} for the β-phase and 1234 cm^{-1} for the γ- phase [35]. For wire-bar coated samples, neither of these two characteristic peaks were observed. Addition of Fe_3O_4 nanoparticles in PVDF does not induce β phase formation.

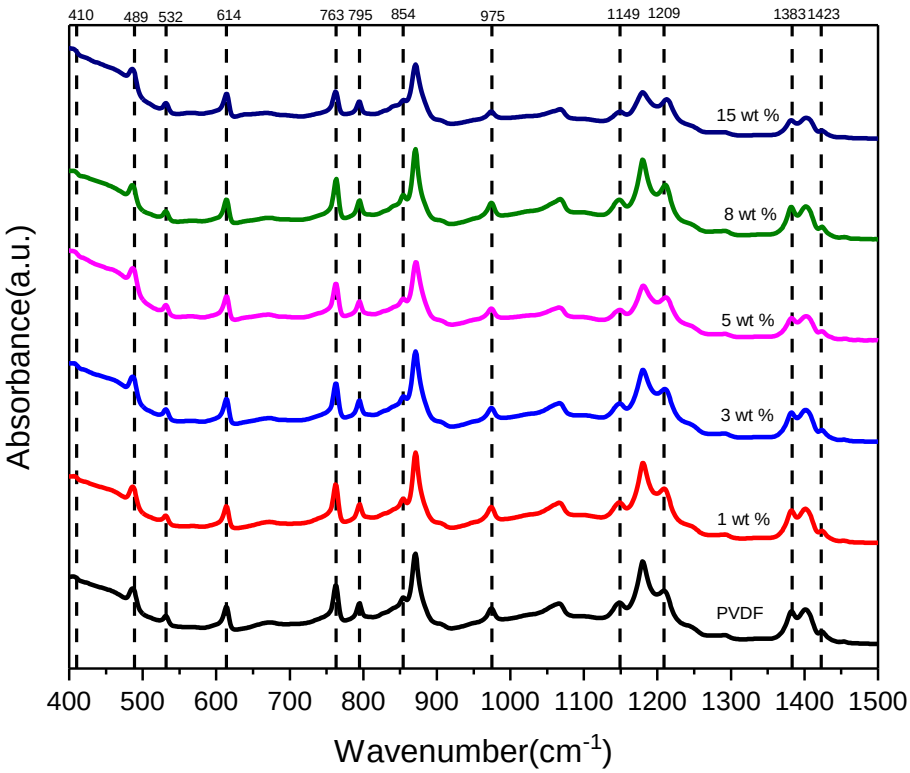

Figure 18. FTIR spectra of pure PVDF and PVDF nanocomposite films with different content of Fe_3O_4 nanoparticles.

5.1.3 Differential Scanning Calorimetry

Differential scanning calorimetry (DSC) is a thermoanalytical technique that has been a complementary method to FTIR and XRD and also used for the identification of the crystalline structure of polymer. The DSC thermograms under heating and cooling conditions of the neat PVDF and PVDF nanocomposites are presented in Figure 19. The degree of crystallinity was determined using the following equation [46]:

$$X_c = \frac{\Delta H}{x\Delta H_\alpha + y\Delta H_\beta} \quad (5)$$

where ΔH is the melting enthalpy of the sample under consideration; ΔH_α and ΔH_β are the melting enthalpy of a 100% crystalline sample of α-PVDF and β-PVDF respectively, and x and y are the amount of the α- and β-phase present in the sample. In this study, a value of 93.07 Jg^{-1} and 103.4 Jg^{-1} [13] was used for ΔH_α and ΔH_β respectively.

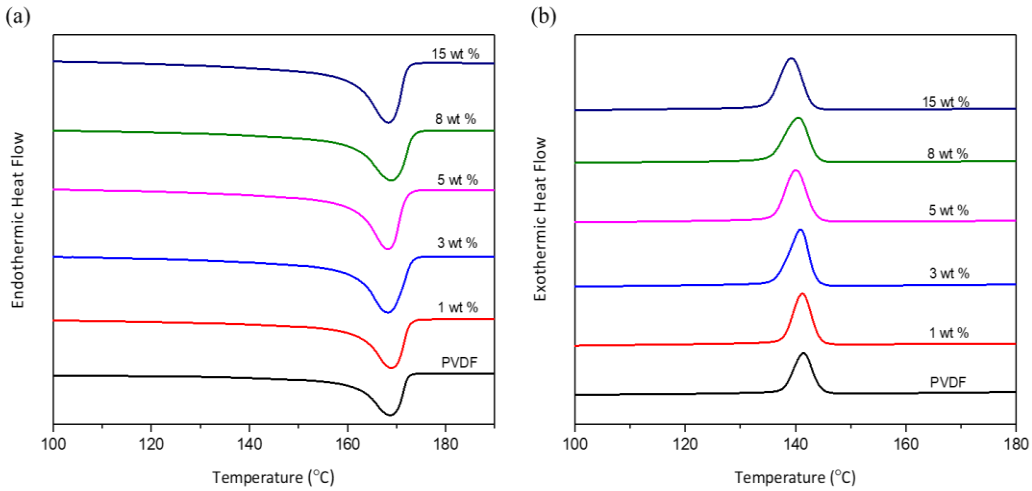

Figure 19. DSC thermograms under (**a**) heating and (**b**) cooling conditions of pure PVDF and PVDF nanocomposite films with different content of Fe_3O_4 nanoparticles.

From the DSC measurements, no remarkable changes in melting temperature and crystallization temperature in PVDF nanocomposite have been observed. We have already used FTIR to establish that all the samples exhibit α-phase. Therefore, it is expected that nanocomposite will show melting peaks of α-phase PVDF 167 °C. In our case, the melting peaks were around 168°C for all samples. However, β-phase PVDF presents a similar melting temperature with α-phase PVDF [10]. Therefore, DSC measurement can not be used to distinguish α- and β-phase, but can be used to calculate the crystalline percentage of the film. Table 5.1 presents the values of melting peak of the thermograms and the crystallinity content of the samples. It

shows the addition of Fe_3O_4 nanoparticles cause the decreasing of crystallinity and the report [47] also had the same observation.

Sample	T_m(°C)	T_c(°C)	X_c(%)
Neat PVDF	168.49	141.3	49.87
1 wt %	168.69	140.2	49.28
3 wt %	167.97	140.9	51.50
5 wt %	167.93	140.0	39.27
8 wt %	168.66	140.5	41.09
15 wt %	167.99	139.1	32.54

Table 2. T_m, T_c and X_c values of PVDF and PVDF: Fe_3O_4 nanocomposite films with different content of Fe_3O_4 nanoparticles.

5.1.4 Thermogravimetric Analysis

Thermogravimetric analysis techniques measure the mass of a sample over the time as a function of temperature and it can used to determines temperature and weight change of decomposition reactions. Figure 20 presents TGA thermograms of PVDF and PVDF nanocomposites. As indicated in the figure, the degradation of PVDF nanocomposites which is reflected with the major weight loss occurs in the range from 400 °C to 500 °C. The onset degradation temperature of pure PVDF was around 467 °C. However, the introduction of Fe_3O_4 nanoparticles increased the initial decomposition temperature and shifted to 482 °C, 481°C, 484 °C, 478 °C and 484°C in the case of 1 wt %, 3 wt %, 5 wt %, 8 wt % and 15 wt % Fe_3O_4 nanoparticles added. This indicates that the thermal stability of PVDF nanocomposites is significantly enhanced compared to pure PVDF. The enhancement of thermal stability may be explained by the better packing of PVDF nanocomposite with Fe_3O_4 nanoparticles loading compared to pure PVDF. Moreover, nano-incorporation and interaction between the Fe_3O_4 nanoparticles and PVDF matrix may also enhance the thermal stability [48].

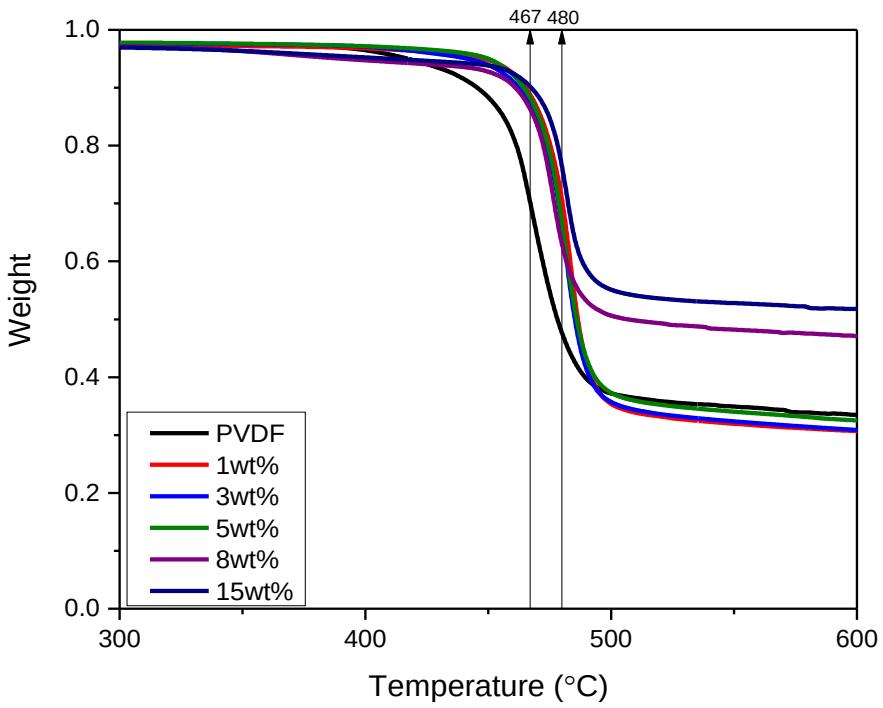

Figure 20. TGA thermograms of PVDF and PVDF nanocomposites with different content of Fe_3O_4 nanoparticles.

5.1.5 Ferroelectric Properties

The room temperature ferroelectric (D-E) hysteresis loops of pure PVDF and PVDF: Fe_3O_4 nanocomposite films with different contents of Fe_3O_4 nanoparticle are shown in Figure 21. As indicated in the figure, all the samples behave paraelectric α phase. At the same time, the inclusion of Fe_3O_4 nanoparticles reduce electric breakdown field. After applying a high electric field of about 250 MV/m, δ phase formation has not been observed. For high concentration of nanoparticles, electric breakdown filed reduces dramatically. One of the possible reason is the rotation of molecular chain was prohibited due to the existence of nanoparticles inside of polymer matrix. Another possible reason is the resistivity of Fe_3O_4 is 0.01 Ohm cm at room temperature and present metallic character [42]. Therefore, the addition of Fe_3O_4 nanoparticles decreases the overall resistivity in the system. Moreover, there are

some oxygen vacancies in Fe_3O_4 could also lead to the increase of leakage current [43].

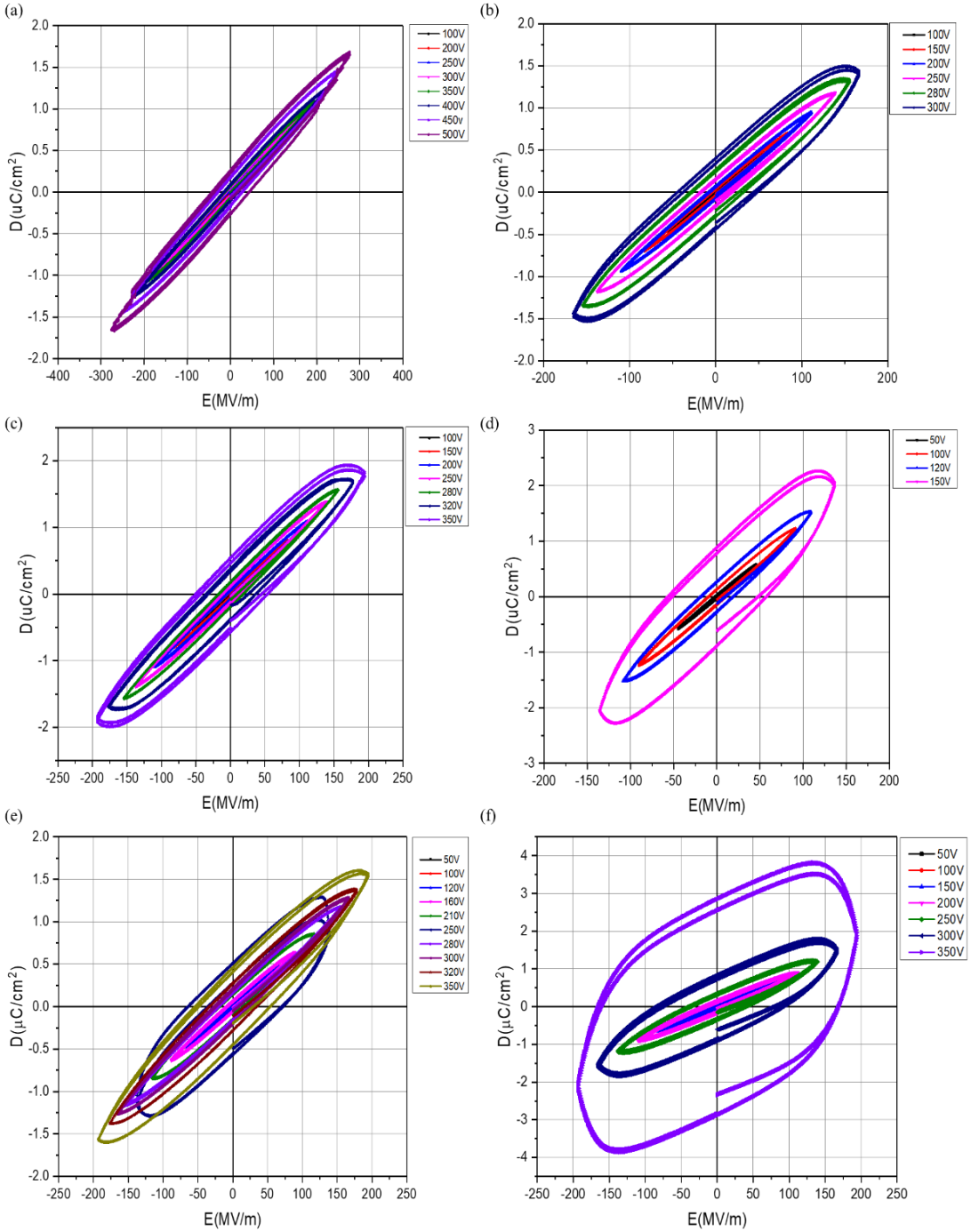

Figure 21. Electric filed dependent polarization. (**a**) Pure PVDF. (**b-f**) PVDF: Fe_3O_4 nanocomposite films with different nanoparticles content 1 wt %, 3 wt %, 5 wt %, 8 wt % and 15 wt % respectively.

5.1.6 Dielectric Properties

Dielectric properties of wire-bar coated PVDF: Fe_3O_4 nanocomposite thick films were characterized using Novocontrol control dielectric spectrometer. Figure 22 shows the dependence of the dielectric properties of the PVDF: Fe_3O_4 nanocomposite films with nanoparticle content up to 8 wt % on the frequency range between 10^{-1} and 10^{7} Hz at room temperature and atmospheric pressure.

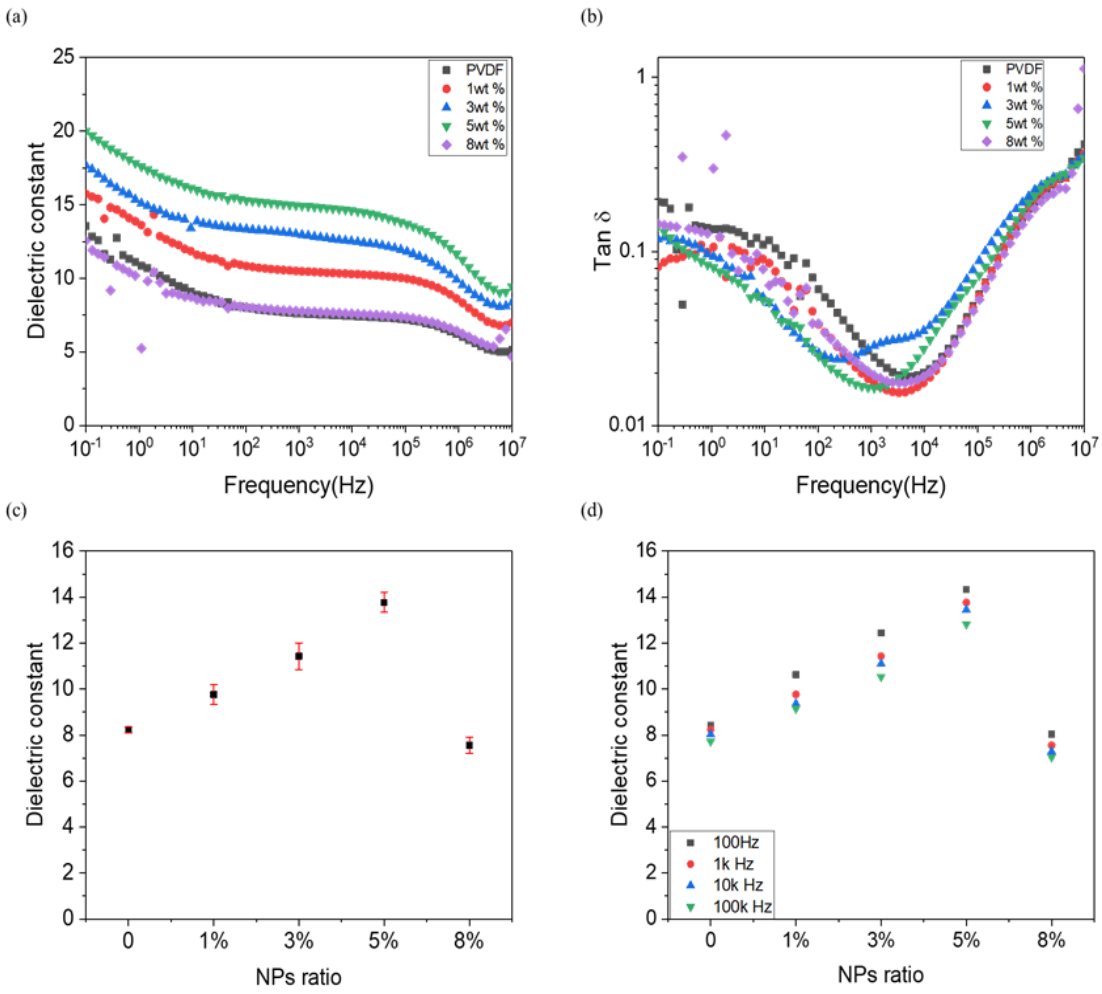

Figure 22. Dielectric properties of wire-bar coated PVDF: Fe_3O_4 nanocomposite films. (**a**) Dielectric constant and (**b**) loss tangent with different nanoparticles content. (**c**) Dielectric constant at 1 kHz as a function of nanoparticles content and (**d**) dielectric constant of PVDF nanocomposite films as a function of composition at 100 to 100 kHz.

As it can be seen in Figure 22 a, a significant improvement in dielectric constant up to 5 wt % the PVDF nanocomposite film in comparison to pure PVDF film was observed. The average dielectric constant values were plotted versus nanoparticle content at 1 kHz and the error bars represent the standard deviation of the mean dielectric constant (Figure 22 c). The dielectric constant of pure PVDF film was 8 at 100 Hz, with values increasing to about 10 for 1 wt % nanocomposite films, to about 12 for 3 wt % nanocomposite films. A maximum dielectric constant of 14 is observed for 5 wt % nanocomposite films, while maintaining low loss. Further doping of Fe_3O_4 nanoparticles decreases the value of dielectric constant. The observed behavior is consistent with the reported data [18]. Generally, there are several reasons responsible for the observed increase in dielectric constant of nanocomposites. The first one is Maxwell-Wagner-Sillars (MWS) polarization effect [49] which occurs in heterogeneous medium consisting of phases with different permittivity and conductivity due to accumulation of the mobile charges at an interface between electrode and nanocomposite films. This effect can be observed particularly in the low frequency range [30]. At low Fe_3O_4 nanoparticles concentration, the Fe_3O_4 nanoparticles are well separated from each other with no effective interaction between them. With increasing Fe_3O_4 nanoparticles content, the number of nanoparticles and their interfacial area per unit volume increases with a decrease in the interparticle distance which improves the interfacial polarization [50]. Higher doping concentrations of the Fe_3O_4 nanoparticles increase void space and without sufficient matrix polymer to fill the space between particles, the interstitial void space (with a dielectric constant of 1) increases [51], resulting in a decrease in dielectric constant. Paper [44] also reported the enhancement of the dielectric constant with low dielectric constant fillers. The model they used is based on the electric multilayer, the surface-area-to-volume plays an important role on the overall polarization response. An optimal distance of the surface of the fillers leads to high local dielectric constant. However, an increased or decreased distance between the

nearest nanofillers, both of which will result in a decreased dielectric constant. Another possible reason is the formation of a network of micro-capacitors in the nanocomposite due to the inclusion of nanoparticles. When the nanoparticles are loaded into PVDF matrix, they could act as micro-capacitor and lead to an overall increase in dielectric constant of nanocomposites compared with pure PVDF [52]. Figure 22 b shows frequency dependence of loss tangent (tan δ) of PVDF: Fe_3O_4 nanocomposite films and pure PVDF film. As shown from the figure, the increase in dielectric loss with decreasing frequency at the low frequency region ($f < 10^3\ Hz$) is mainly dominated by dc conductivity [50]. It is interesting to note that the dielectric losses of PVDF nanocomposite were suppressed in the low frequency range ($f < 10^3\ Hz$) with respect to pure PVDF which may be explained by the low dc conductivity and decreased crystallinity in PVDF: Fe_3O_4 nanocomposites. However, at the high frequency region ($f > 10^3\ Hz$), both micro-Brownian moments of the amorphous chain segments and molecular motion on the interfaces can attribute to dielectric loss [20].

5.2 Drop cast PVDF: Fe_3O_4 Nanocomposite Thick Films

The nanocomposite solution used is the same solution with wire-bar coated films. Free-standing films with 50-90 μm were prepared by spreading the suspension on clean glass substrates. Solvent evaporation was performed inside the vacuum oven at a temperature of 60 °C for 24 h. The temperature of 60 °C was chosen in order to obtain β-phase PVDF. Pure PVDF films were also prepared under identical conditions for comparison.

5.2.1 Morphology Characterization

The microstructure of the prepared films was analyzed by scanning electron microscopy (SEM). Figure 23 shows the SEM images of PVDF nanocomposite

films with 5 wt % Fe_3O_4 nanoparticles. The main relevant microstructural feature of the sample is the following: the films display spherulites with a high degree of porosity and high roughness. Most of the nanoparticles aggregated into clusters and were embedded deeply in the film.

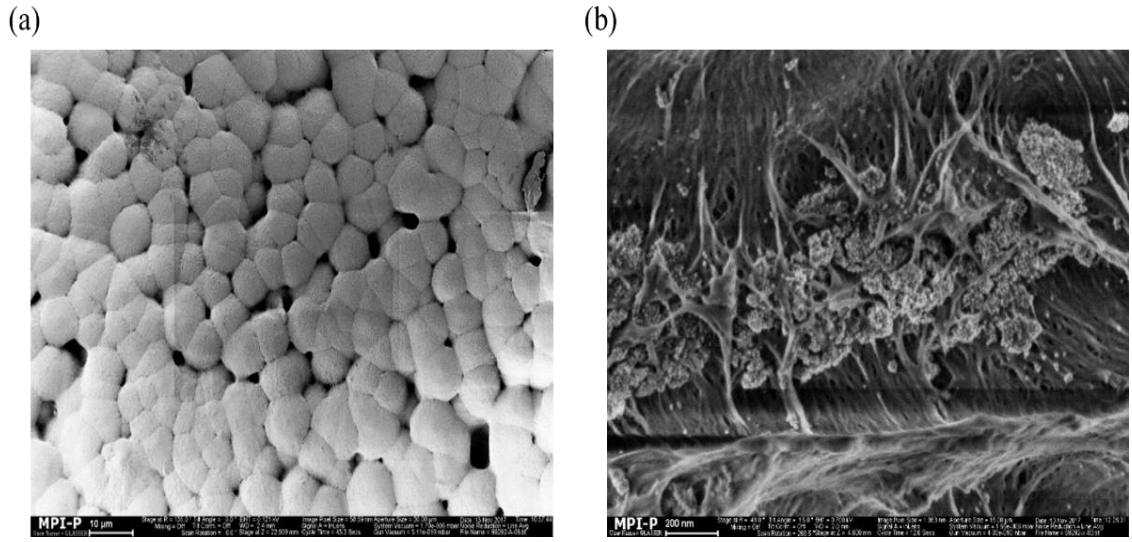

Figure 23. SEM images of 5 wt % PVDF nanocomposite film. (a) Top view and (b) cross section

5.2.2 Fourier Transformed Infrared Spectroscopy

FTIR spectra of pure PVDF film and PVDF: Fe_3O_4 nanocomposite films were presented in Figure 24. Due to the similarity of the β- and γ- phase specific conformations, some bands are simultaneously common to the β- and γ- phase. That is for example, 512 cm^{-1} is characteristic band of γ- phase and it is very close to 510 cm^{-1} of β-phase characteristic band [53] . Therefore, it leads to contradictory opinion regarding the identification of β- and γ- phase [54]. α-phase PVDF is easily distinguished as it exhibits a large number of characteristic bands which are the exclusive for this phase, such as 410, 489, 532, 614, 763, 795, 854, 975, 1179, 1209, 1383 and 1423 cm^{-1}. Report [45] provides identification method of the β- and γ-phase based on exclusive peaks. There are only two exclusive bands of 1275 cm^{-1}

for the β-phase and 1234 cm^{-1} for the γ- phase. If the FTIR spectra exhibit exclusive peak 1275 $cm^{-1}$and without 1234 cm^{-1} band, the sample is considered as the β-phase. On the contrary, if 1234 cm^{-1} band are showed together with the absence of the 1275 cm^{-1}, the sample is considered as the γ- phase. In our case, all the drop cast samples show exclusive peak 1234 cm^{-1}. At the same time, exclusive peak 1275 cm^{-1} of β-phase is not found. Characteristic bands at 431, 482, 510, 811 and 833 cm^{-1} also correspond to γ phase. In fact, none of the characteristic α-phase absorption bands can be observed in the drop cast PVDF: Fe_3O_4 nanocomposite films. The measurement results imply the inclusion of nanoparticles does not affect the PVDF crystalline phase, and the processing conditions are the main reason for the formation of α-, β- or γ-phase. This finding is consistent with the report [59].

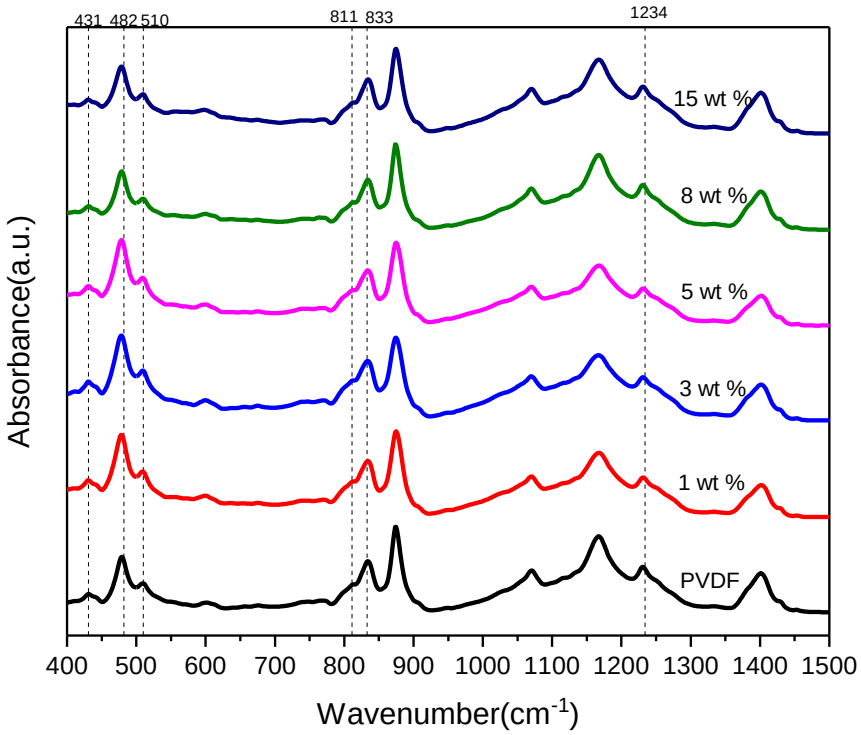

Figure 24. FTIR spectra of pure PVDF and PVDF: Fe_3O_4 nanocomposite films processed by drop casting.

5.2.3 X-ray Diffraction

The XRD patterns of neat PVDF and PVDF nanocomposite films are presented in Figure 25. All α, β or γ phases have an intense peak around 20°, some of them are exclusive of each other. In general, the β phase can be characterized by the presence of only one peak at 20° in the whole XRD spectra [55]. However, the identification of γ phase still have problems. This is due to samples containing the γ phase that always contain a large amount of the α phase, generally, γ-phase presents a superposition of peaks at 18.5° and 19.2° and a more intense peak at 20.04° [53]. The combination of XRD result with FTIR technique (explained in previous section) confirms the addition of Fe_3O_4 does not affect polymer phase.

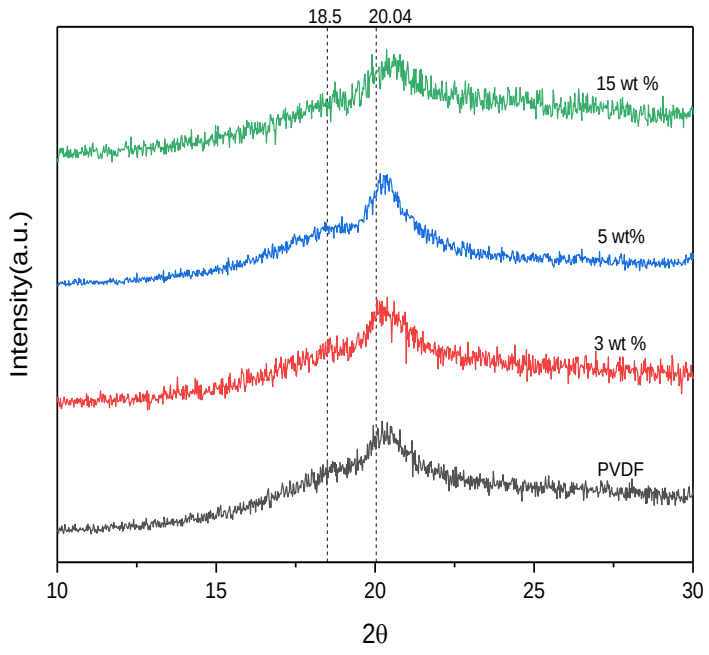

Figure 25. X-ray diffraction patterns of pure PVDF and PVDF nanocomposite films containing various amounts of Fe_3O_4 nanoparticles.

5.2.4 Dielectric Properties

Figure 26 shows the frequency-dependent dielectric constant and dielectric loss tangent of drop cast PVDF nanocomposites at room temperature. The result is in

good agreement with wire-bar coated samples. One can see from Figure 26 (a) that the frequency dependence of the dielectric properties of the drop cast nanocomposite films shows similar behavior to the wire-bar coated PVDF: Fe_3O_4 nanocomposite films. It can be found that the dielectric constant of the PVDF: Fe_3O_4 nanocomposite films increases with gradually increasing nanoparticles content. The maximum dielectric constant of the PVDF: Fe_3O_4 nanocomposite films is 14 when the content of Fe_3O_4 nanoparticles is 5 wt %. In comparison with pure PVDF ($\varepsilon = 8$), the dielectric constant of the composite is nearly 2 times higher. This indicates that incorporating Fe_3O_4 nanoparticles into the polymer matrix results in an enhancement in dielectric constant. The significant increase in dielectric constant of PVDF: Fe_3O_4 nanocomposite films can be attributed to the formation of a quantity of micro-capacitors. With increased nanoparticles concentration, more micro-capacitance structures are constructed and greater interfacial areas are introduced in the composite, resulting in higher dielectric constant relative to that of pure PVDF. In addition, charges can be accumulated at the interfaces between Fe_3O_4 nanoparticles and polymer matrix due to their different dielectric constant as well as conductivity, thus interfacial polarization (Maxwell-Wagner-Sillars effect) can also makes a remarkable contribution to the increase in dielectric constant of PVDF: Fe_3O_4 nanocomposites in the low-frequency range [56]. The decrease in dielectric constant of PVDF nanocomposites with frequency may be explained that it becomes difficult for dipoles to execute the flipping motion and accumulation process needs to have a relatively long time with frequency increasing. Therefore there would be losses arising due to the dipolar relaxation [3]. All the drop cast samples show the similar dielectric loss tangent compared with pure PVDF. In fact, many works reported that the nanocomposite exhibit lower dielectric loss tangent at high frequencies [57]. Since the dielectric loss at higher frequencies mainly originates from the electrical conduction and dipolar polarization. The possible reason for the

decrease of dielectric loss in the nanocomposites can be the inorganic fillers limit the macromolecular movement [58].

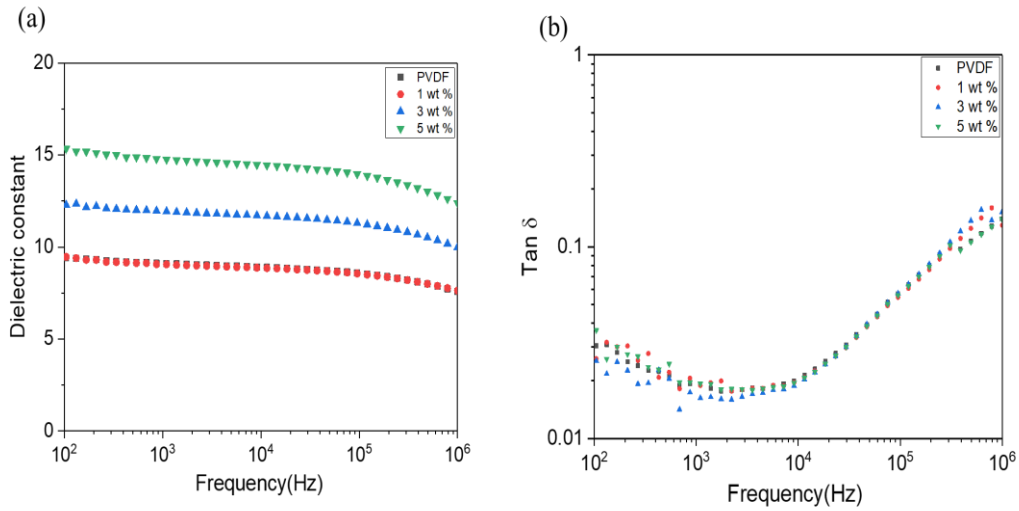

Figure 26. (**a**) Frequency dependence of dielectric constant and (**b**) dielectric loss tangent of the PVDF: Fe_3O_4 nanocomposite films processed by drop casting.

5.3 Summary

Nanocomposite films of PVDF: Fe_3O_4 with favorable dielectric properties are fabricated through wire-bar coating and drop casting methods respectively. The addition of nanoparticles does not affect the PVDF crystalline phase, and the processing conditions are the main reason for the formation of α-, β- or γ-phase. This finding is consistent with the report [59]. A significant improvement of dielectric constant with low dielectric loss are observed in both bar-coated and drop cast samples. A dielectric constant value of 14 and a loss tangent of 0.02 at 1 kHz were measured with 5 wt % Fe_3O_4 nanoparticles loaded. The polymeric crystalline phase is not relevant for the dielectric properties of nanocomposites. The distribution and content of nanoparticles plays a major role in dielectric behavior.

Chapter 6

6 Conclusions and Outlook

6.1 Conclusions

In this thesis, firstly the suitable processing condition was determined to get transparent, flat and smooth films. The films processed at an elevated temperature and low relative humidity exhibited low roughness. In order to investigate the effect of thermal treatment, after deposition of the film, the samples were received melt quenching with subsequent annealing and only annealing treatment. From the experimental results, melt quenching with subsequent annealing samples showed high breakdown strength.

PVDF: Fe_3O_4 nanocomposite thin films were prepared by spin coating at 100 °C, the thickness was around 300nm. Ferroelectric properties and dielectric properties were investigated. The addition of nanoparticles did not enhance ferroelectric properties and dielectric properties. The possible reason is Fe_3O_4 nanoparticles aggregated into clusters causing more defects in polymer matrix which was confirmed by AMF and SEM measurements and affect the physical properties of PVDF nanocomposite thin films.

PVDF: Fe_3O_4 nanocomposite thick films were fabricated by wire-bar coating and drop casting respectively. The frequency dependent dielectric constant and the loss tangent were studied for the PVDF nanocomposite thick films. Inclusion of Fe_3O_4 nanoparticles in PVDF matrix significantly enhances dielectric properties of the polymer. A dielectric constant value of 14 and loss tangent of 0.02 at 10^3 Hz were measured at a Fe_3O_4 nanoparticle concentration of 5 wt %. Possible mechanisms

responsible for these observed improvements in dielectric properties have been discussed. At the same time, crystalline phase of PVDF: Fe_3O_4 nanocomposite films was studied by FTIR and XRD, the addition of Fe_3O_4 nanoparticles did not induce β phase. The processing conditions are the main reason for the formation of α-, β- or γ-phase. The polymeric crystalline phase is not relevant for the dielectric properties of nanocomposites. The distribution and content of nanoparticles plays a major role in dielectric behavior. All these results suggest that this polymer nanocomposite material system is promising candidates for energy storage and multiferroic magnetoelectric applications.

6.2 Outlook

The experimental results suggest the uniform distribution of nanoparticles in PVDF polymer matrix without particle agglomeration plays an important role for the physical properties of PVDF nanocomposite. As a future work, nanoparticle distribution in polymer matrix can be controlled through surface modification of nanoparticles. By tailoring interactions between nanoparticles and polymer matrix, improved dielectric and ferroelectric properties can be achieved. The magnetoelectric effect will be investigated in PVDF: Fe_3O_4 nanocomposites.

Bibliography

[1] M. F. Nicola A. Spaldin, "The Renaissance of Magnetoelectric Multiferroics," *Science (80-.).*, vol. 309, no. July, pp. 391–392, 2005.

[2] M. Fiebig, "Revival of the magnetoelectric effect," *J. Phys. D. Appl. Phys.*, vol. 38, no. 8, 2005.

[3] G. Suresh, S. Jatav, M. S. Ramachandra Rao, and D. K. Satapathy, "Enhancement of dielectric and ferroelectric properties in cobalt ferrite doped poly(vinylidene fluoride) multiferroic composites," *Mater. Res. Express*, vol. 4, no. 7, 2017.

[4] T. Prabhakaran and J. Hemalatha, "Poly (vinylidene fluoride) -Based Magnetoelectric Polymer Nanocomposite Films," *Magnetoelectric Polym. Compos. Fundam. Appl.*, 2017.

[5] P. Martins and S. Lanceros-Méndez, "Polymer-based magnetoelectric materials," *Adv. Funct. Mater.*, vol. 23, no. 27, pp. 3371–3385, 2013.

[6] K. M. Rabe, C. H. Ahn, J. M.-M. Triscone, M. Dawber, and C. Lichtensteiger, *Physics of Ferroelectrics*, vol. 105, no. 2007. 2007.

[7] Q. X. Chen and P. A. Payne, "Industrial applications of piezoelectric polymer transducers," *Meas. Sci. Technol.*, vol. 6, no. 3, pp. 249–267, 1995.

[8] N. Tsutsumi, X. Bai, and W. Sakai, "Towards nonvolatile memory devices based on ferroelectric polymers," *AIP Adv.*, vol. 2, no. 1, 2012.

[9] R. Gregorio and E. M. Ueno, "Effect of crystalline phase, orientation and temperature on the dielectric properties of poly (vinylidene fluoride) (PVDF)," *J. Mater. Sci.*, vol. 34, no. 18, pp. 4489–4500, 1999.

[10] R. Crecorio and M. Cestari, "Effect of Crystallization Temperature on the Crystalline Phase Content and Morphology of Poly (vinylidene Fluoride)," *J. Polym. Sci. Part B Polym. Phys.*, vol. Vol. 32, pp. 859–870, 1994.

[11] M. Li, H. J. Wondergem, M. J. Spijkman, K. Asadi, I. Katsouras, P. W. M. Blom, and D. M. De Leeuw, "Revisiting the δ-phase of poly(vinylidene fluoride) for solution-processed ferroelectric thin films," *Nat. Mater.*, 2013.

[12] A. J. Lovinger, "Ferroelectric Polymers," *Science (80-.).*, vol. 220, no. 4602, pp. 1115–1121, 1983.

[13] S. Lanceros-Méndez, J. F. Mano, A. M. Costa, and V. H. Schmidt, "Ftir and Dsc Studies of Mechanically Deformed B-Pvdf Films," *J. Macromol. Sci. Part B*, vol. 40, no. 3–4, pp. 517–527, 2001.

[14] V. Sencadas, R. Gregorio Filho, and S. Lanceros-Mendez, "Processing and characterization of a novel nonporous poly(vinilidene fluoride) films in the β phase," *J. Non. Cryst. Solids*, vol. 352, no. 21–22, pp. 2226–2229, 2006.

[15] B. H. Fan, J. W. Zha, D. Wang, J. Zhao, and Z. M. Dang, "Size-dependent low-frequency dielectric properties in the BaTiO 3/poly(vinylidene fluoride) nanocomposite films," *Appl. Phys. Lett.*, vol. 100, no. 1, 2012.

[16] M. Sharma, G. Madras, and S. Bose, “Contrasting Effects of Graphene Oxide and Poly(ethylenimine) on the Polymorphism in Poly(vinylidene fluoride),” *Cryst. Growth Des.*, vol. 15, no. 7, pp. 3345–3355, 2015.

[17] L. Priya and J. P. Jog, “Poly(vinylidene fluoride)/clay nanocomposites prepared by melt intercalation: Crystallization and dynamic mechanical behavior studies,” *J. Polym. Sci. Part B Polym. Phys.*, vol. 40, no. 15, pp. 1682–1689, 2002.

[18] R. Gonçalves, P. M. Martins, C. Caparrós, P. Martins, M. Benelmekki, G. Botelho, S. Lanceros-Mendez, A. Lasheras, J. Gutiérrez, and J. M. Barandiarán, “Nucleation of the electroactive β-phase, dielectric and magnetic response of poly(vinylidene fluoride) composites with Fe2O 3 nanoparticles,” *J. Non. Cryst. Solids*, vol. 361, no. 1, pp. 93–99, 2013.

[19] J. Li, S. Il Seok, B. Chu, F. Dogan, Q. Zhang, and Q. Wang, “Nanocomposites of ferroelectric polymers with TiO_2 nanoparticles exhibiting significantly enhanced electrical energy density,” *Adv. Mater.*, vol. 21, no. 2, pp. 217–221, 2009.

[20] L. Yang, J. Qiu, H. Ji, K. Zhu, and J. Wang, “Enhanced dielectric and ferroelectric properties induced by TiO_2@MWCNTs nanoparticles in flexible poly(vinylidene fluoride) composites,” *Compos. Part A Appl. Sci. Manuf.*, vol. 65, pp. 125–134, 2014.

[21] M. Arjmand, S. Sadeghi, M. Khajehpour, and U. Sundararaj, “Carbon nanotube/graphene nanoribbon/polyvinylidene fluoride hybrid nanocomposites: Rheological and dielectric properties,” *J. Phys. Chem. C*, vol. 121, no. 1, pp. 169–181, 2017.

[22] P. Martins, R. Gonçalves, S. Lanceros-Mendez, A. Lasheras, J. Gutiérrez, and J. M. Barandiarán, “Effect of filler dispersion and dispersion method on the piezoelectric and magnetoelectric response of $CoFe_2O_4$/P(VDF-TrFE) nanocomposites,” *Appl. Surf. Sci.*, vol. 313, pp. 215–219, 2014.

[23] D. Bhadra, S. C. Sarkar, and B. K. Chaudhuri, “RSC Advances Enhanced dielectric and ferroelectric properties in NaTNO / PVDF nanocomposites : a new flexible material for capacitor application,” *RSC Adv.*, vol. 5, no. December 2016, pp. 36924–36932, 2015.

[24] M. Yang, H. Zhao, D. He, C. Hu, H. Chen, and J. Bai, “Carbon coated boron nitride nanosheets for polymer nanocomposites with enhanced dielectric performance,” *Materials (Basel).*, vol. 10, no. 7, 2017.

[25] P. Thomas, S. Satapathy, K. Dwarakanath, and K. B. R. Varma, “Dielectric properties of poly (vinylidene fluoride)/$CaCu_3Ti_4O_{12}$ nanocrystal composite thick films,” *Express Polym. Lett.*, vol. 4, no. 10, pp. 632–643, 2010.

[26] C. Zhang, Q. Chi, J. Dong, Y. Cui, X. Wang, L. Liu, and Q. Lei, “Enhanced dielectric properties of poly(vinylidene fluoride) composites filled with nano iron oxide-deposited barium titanate hybrid particles,” *Sci. Rep.*, vol. 6, no. June, pp. 4–12, 2016.

[27] H. Luo, D. Zhang, C. Jiang, X. Yuan, C. Chen, and K. Zhou, “Improved dielectric properties and energy storage density of poly(vinylidene fluoride-co-hexafluoropropylene) nanocomposite with hydantoin epoxy resin coated $BaTiO_3$,” *ACS Appl. Mater. Interfaces*, vol. 7, no. 15, pp. 8061–8069, 2015.

[28] A. Toor, H. So, and A. P. Pisano, “Improved dielectric properties of polyvinylidene fluoride nanocomposite embedded with poly(vinyl pyrrolidone) coated gold nanoparticles,” *ACS Appl. Mater. Interfaces*, p. acsami.6b13900, 2017.

[29] K. Meeporn, P. Thongbai, T. Yamwong, and S. Maensiri, “Greatly enhanced dielectric permittivity in $La_{1.7}Sr_{0.3}NiO_4$/poly(vinylidene fluoride) nanocomposites that retained a low loss tangent,” *RSC Adv.*, vol. 7, no. 28, pp. 17128–17136, 2017.

[30] F. He, S. Lau, H. L. Chan, and J. Fan, “High dielectric permittivity and low percolation threshold in nanocomposites based on poly(vinylidene fluoride) and exfoliated graphite nanoplates,” *Adv. Mater.*, vol. 21, no. 6, pp. 710–715, 2009.

[31] X. Huang, P. Jiang, and L. Xie, “Ferroelectric polymer/silver nanocomposites with high dielectric constant and high thermal conductivity,” *Appl. Phys. Lett.*, vol. 95, no. 24, pp. 1–4, 2009.

[32] M. Panda, V. Srinivas, and A. K. Thakur, “On the question of percolation threshold in polyvinylidene fluoride/nanocrystalline nickel composites,” *Appl. Phys. Lett.*, vol. 92, no. 13, pp. 10–13, 2008.

[33] P. Anithakumari, B. P. Mandal, E. Abdelhamid, R. Naik, and A. K. Tyagi, “Enhancement of dielectric, ferroelectric and magneto-dielectric properties in PVDF–$BaFe_{12}O_{19}$ composites: a step towards miniaturizated electronic devices,” *RSC Adv.*, vol. 6, no. 19, pp. 16073–16080, 2016.

[34] J. Fu, Y. Hou, M. Zheng, Q. Wei, M. Zhu, and H. Yan, “Improving Dielectric Properties of PVDF Composites by Employing Surface Modified Strong Polarized $BaTiO_3$ Particles Derived by Molten Salt Method,” *ACS Appl. Mater. Interfaces*, vol. 7, no. 44, pp. 24480–24491, 2015.

[35] F. Wang, D. Zhou, and S. Gong, “Dielectric behavior of TiC-PVDF nanocomposites,” *Phys. Status Solidi - Rapid Res. Lett.*, vol. 3, no. 1, pp. 22–24, 2009.

[36] H. Sharifi Dehsari, A. Halda Ribeiro, B. Ersöz, W. Tremel, G. Jakob, and K. Asadi, “Effect of precursor concentration on size evolution of iron oxide nanoparticles,” *CrystEngComm*, vol. 19, no. 1, pp. 6694–6702, 2017.

[37] H. Sharifi Dehsari, M. Heidari, A. Halda Ribeiro, W. Tremel, G. Jakob, D. Donadio, R. Potestio, and K. Asadi, “Combined Experimental and Theoretical Investigation of Heating Rate on Growth of Iron Oxide Nanoparticles,” *Chem. Mater.*, vol. 29, no. 22, pp. 9648–9656, 2017.

[38] M. Stewart, M. G. Cain, and D. Hall, “Ferroelectric Hysteresis Measurement & Analysis,” *NPL Rep. C.*, no. May, pp. 1–57, 1999.

[39] M. Li, I. Katsouras, C. Piliego, G. Glasser, I. Lieberwirth, P. W. M. Blom, and D. M. de Leeuw, "Controlling the microstructure of poly(vinylidene-fluoride) (PVDF) thin films for microelectronics," *J. Mater. Chem. C*, vol. 1, no. 46, p. 7695, 2013.

[40] H. S. Dehsari, J. J. Michels, and K. Asadi, "Processing of ferroelectric polymers for microelectronics: from morphological analysis to functional devices," *J. Mater. Chem. C*, vol. 5, pp. 10490–10497, 2017.

[41] C. E. Murphy, L. Yang, S. Ray, L. Yu, S. Knox, and N. Stingelin, "Wire-bar coating of semiconducting polythiophene/insulating polyethylene blend thin films for organic transistors," *J. Appl. Phys.*, vol. 110, no. 9, 2011.

[42] R. Prakash, R. J. Choudhary, L. S. Sharath Chandra, N. Lakshmi, and D. M. Phase, "Electrical and magnetic transport properties of Fe_3O_4 thin films on a GaAs(100) substrate," *J. Phys. Condens. Matter*, vol. 19, no. 48, 2007.

[43] O. D. Jayakumar, B. P. Mandal, J. Majeed, G. Lawes, R. Naik, and A. K. Tyagi, "Inorganic–organic multiferroic hybrid films of Fe_3O_4 and PVDF with significant magneto-dielectric coupling," *J. Mater. Chem. C*, vol. 1, no. 23, p. 3710, 2013.

[44] Y. Thakur, T. Zhang, C. Iacob, T. Yang, J. Bernholc, L. Q. Chen, J. Runt, and Q. M. Zhang, "Enhancement of the dielectric response in polymer nanocomposites with low dielectric constant fillers," *Nanoscale*, vol. 3, pp. 10992–10997, 2017.

[45] X. Cai, T. Lei, D. Sun, and L. Lin, "A critical analysis of the α, β and γ phases in poly(vinylidene fluoride) using FTIR," *RSC Adv.*, vol. 7, no. 25, pp. 15382–15389, 2017.

[46] C. Ribeiro, V. Sencadas, J. L. G. Ribelles, and S. Lanceros-Méndez, "Influence of processing conditions on polymorphism and nanofiber morphology of electroactive poly(vinylidene fluoride) electrospun membranes," *Soft Mater.*, vol. 8, no. 3, pp. 274–287, 2010.

[47] P. Martins, C. M. Costa, and S. Lanceros-Mendez, "Nucleation of electroactive ß-phase poly(vinilidene fluoride) with $CoFe_2O_4$ and $NiFe_2O_4$ nanofillers: A new method for the preparation of multiferroic nanocomposites," *Appl. Phys. A Mater. Sci. Process.*, vol. 103, no. 1, pp. 233–237, 2011.

[48] R. K. Layek, A. K. Das, M. J. Park, N. H. Kim, and J. H. Lee, "Enhancement of physical, mechanical, and gas barrier properties in noncovalently functionalized graphene oxide/poly(vinylidene fluoride) composites," *Carbon N. Y.*, vol. 81, no. 1, pp. 329–338, 2015.

[49] P. Lunkenheimer, V. Bobnar, V. Bobnar, A. V. Pronin, A. V. Pronin, A. I. Ritus, A. A. Volkov, and A. Loidl, "Origin of apparent colossal dielectric constants," *Phys. Rev. B - Condens. Matter Mater. Phys.*, vol. 66, no. 5, pp. 521051–521054, 2002.

[50] P. Thakur, A. Kool, B. Bagchi, S. Das, and P. Nandy, "Effect of in situ synthesized Fe_2O_3 and Co_3O_4 nanoparticles on electroactive β phase

crystallization and dielectric properties of poly(vinylidene fluoride) thin films," *Phys. Chem. Chem. Phys.*, vol. 17, no. 2, pp. 1368–1378, 2015.

[51] Y. N. Hao, K. Bi, S. O'Brien, X. X. Wang, J. Lombardi, F. Pearsall, W. L. Li, M. Lei, Y. Wu, and L. T. Li, "Interface structure, precursor rheology and dielectric properties of $BaTiO_3$ /PVDF–hfp nanocomposite films prepared from colloidal perovskite nanoparticles," *RSC Adv.*, vol. 7, no. 52, pp. 32886–32892, 2017.

[52] P. Fakhri, H. Mahmood, B. Jaleh, and A. Pegoretti, "Improved electroactive phase content and dielectric properties of flexible PVDF nanocomposite films filled with Au- and Cu-doped graphene oxide hybrid nanofiller," *Synth. Met.*, vol. 220, pp. 653–660, 2016.

[53] R. Gregorio, "Determination of the alpha, beta, and gamma crystalline phases of poly(vinylidene fluoride) films prepared at different conditions," *J. Appl. Polym. Sci.*, vol. 100, no. 4, pp. 3272–3279, 2006.

[54] T. Boccaccio, A. Bottino, G. Capannelli, and P. Piaggio, "Characterization of PVDF membranes by vibrational spectroscopy," *J. Memb. Sci.*, vol. 210, no. 2, pp. 315–329, 2002.

[55] P. Martins, A. C. Lopes, and S. Lanceros-Mendez, "Electroactive phases of poly(vinylidene fluoride): Determination, processing and applications," *Prog. Polym. Sci.*, vol. 39, no. 4, pp. 683–706, 2014.

[56] E. El Shafee, M. El Gamal, and M. Isa, "Electrical properties of multi walled carbon nanotubes/ poly(vinylidene fluoride/trifluoroethylene) nanocomposites," *J. Polym. Res.*, vol. 19, no. 1, pp. 1–8, 2012.

[57] L. Xie, X. Huang, K. Yang, S. Li, and P. Jiang, "'Grafting to' route to PVDF-HFP-GMA/$BaTiO_3$ nanocomposites with high dielectric constant and high thermal conductivity for energy storage and thermal management applications," *J. Mater. Chem. A*, vol. 2, no. 15, p. 5244, 2014.

[58] M. Zhu, X. Huang, K. Yang, X. Zhai, J. Zhang, J. He, and P. Jiang, "Energy storage in ferroelectric polymer nanocomposites filled with core-shell structured polymer@$BaTiO_3$ nanoparticles: Understanding the role of polymer shells in the interfacial regions," *ACS Appl. Mater. Interfaces*, vol. 6, no. 22, pp. 19644–19654, 2014.

[59] S. Firmino Mendes, C. M. Costa, V. Sencadas, J. Serrado Nunes, P. Costa, R. Gregorio, and S. Lanceros-Méndez, "Effect of the ceramic grain size and concentration on the dynamical mechanical and dielectric behavior of poly(vinilidene fluoride)/$Pb(Zr_{0.53}Ti_{0.47})O_3$ composites," *Appl. Phys. A Mater. Sci. Process.*, vol. 96, no. 4, pp. 899–908, 2009.

Acknowledgment

I would like to thank my thesis advisor, Dr. Kamal Asadi who gave me this opportunity to do this project. He spent countless hours in the lab explaining and showing me how to do everything and for sacrificing his time to help me. I am very grateful for his scientific advice and knowledge and many insightful discussions and suggestions. I would like to express my deepest appreciation to Hamed Sharifi Dehsari who served as my supervisor and provided invaluable guidance. I always feel I have been extremely lucky to have a supervisor who cared so much about my work, and who responded to my questions and queries so promptly. I wish him further success in his all endeavors.

I express my sincere gratitude to Prof. Uli Lemmer who act as my thesis advisor and has been a great teacher. Prof. Uli Lemmer has always been helpful in providing advice many times during my master study in KSOP. He was and remains my best role model for a scientist, mentor, and teacher.

I would like to express my thanks to Gunnar Glaßer, Verona Maus, Michael Steiert, Frank Keller and Christian Bauer who provided technical support and helped me in handling the instruments. In particular I would like to thank all the group members from Dr. Kamal Asadi for their great support. I enjoyed stimulating research discussions with them.

Finally, I would like to thank my parents for their love and continuous support. Without their encouragement and support, I doubt that I would be in this place today.